**Response to reviews of:**

**Solar geoengineering using solid aerosol in the stratosphere**
**by D. K. Weisenstein[1] and D. W. Keith**
**ACPD-15-11799**

## Response to Anonymous Referee #1

Received and published: 12 May 2015

First we would like to thank the reviewer for a careful reading of our manuscript and many constructive comments that have improved the quality and clarity of the paper. We have added a table to list the model experiments described and an appendix to detail the coagulation and condensation schemes. We added a paragraph on the limitations and inherent size broadening of a discrete sectional bin scheme. We have included a more thorough description of the AER 2-D model's dynamical fields and PSC parameterization and discuss some model comparisons with observations for both aerosols and ozone. We adjusted our RF values in Figures 7 and 13 due to a correction in the albedo adjustment. We added a comparison of ozone change from sulfate geoengineering to that from alumina and diamond geoengineering in Figure 12a. We also replace the unit megatons with terragrams throughout the manuscript. We have added seventeen new references and increased font size and readability of the figures. J. A. Dykema has been added as a co-author (previously recognized in a footnote and acknowledgement) due to his scientific contributions in addressing reviewer questions regarding heating rates and radiative forcing.

Our answers to the reviewer's questions and comments are detailed below, with the reviewer's comments in black and our responses indented and in green.

First I should say I have not evaluated the ozone depletion part of the paper as this falls out of my expertise, and have focused instead on the physical part

of the study. I confess I am not very knowledgeable in fractal aerosols and have not checked the details of the authors' treatment in this study.

Independently of what one may think of the idea of injecting alumina particles in the stratosphere, I think this is, scientifically speaking, a good study. The limitations of the model used (simplified injection mechanism and lack of a plume model, 2D modelling, geometry of aggregates, ozone chemistry and missing feedbacks on the stratospheric circulation and ozone distribution) are highlighted and well discussed in Section 4. The conclusions are clearly explained and the results make physically sense.

I have a few major comments:

The number of monomers in a fractal particle is always a power of 2 as a consequence of the sectional representation that doubles the number of monomers in successive bins. Yet fractal particles of different sizes can coagulate and produce particles with any number of monomers. How is this treated in the model? How much of an assumption is this? Actually fairly little is said on the coagulation scheme for coated and uncoated particles. As this is a new development, it would be useful to describe it in an Appendix. Likewise a better description of the other aspects of the scheme like condensation of sulphuric acid on the particles is needed.

> We agree with the reviewer that a more comprehensive description of this aspect of the model was need. We have added Appendix A to explain the coagulation and condensation schemes. We also added a paragraph in section 4.1 to discuss limitations due to aerosol size binning.

It seems that all "radiative forcing" estimates are for SW effects only (at least this is what I understand from page 11816, lines 10-12). If this is the case, this should be made explicit and justified. This said neglecting the LW (positive) radiative forcing is hardly justifiable given that it can vary significantly between the different particle types (as the authors explain themselves).

> Figures 6 and 7 present calculations accounting for only shortwave effects on radiative forcing. We have made this explicit in the text and figure captions. For purposes of geoengineering, we believe shortwave

radiative forcing is the most appropriate metric for comparing different geoengineering methods, especially for a model without interactive dynamics. Changes in stratospheric temperature in response to changes in radiative heating rates may lead to more substantial adjustments in longwave radiative forcing relative to shortwave radiative forcing. Thus the instantaneous longwave radiative forcing is a more ambiguous indicator of changes in surface temperature, which geoengineering attempts to offset. This problem is complex and will be dealt with in a future paper by John Dykema of our group. However, we have made a preliminary calculation of the LW vs SW RF and find that the LW is about 10% of the SW for alumina and is negligible for diamond. We have added the following to our discussion of radiative forcing: "We choose to present only shortwave radiative forcing as more relevant to geoengineering intended to offset surface warming after atmospheric adjustments. However, the longwave radiative forcing is only about 10% of the shortwave RF for alumina, though of opposite sign, and is negligible for diamond."

The paragraphs on heating rates are also unclear and possibly incorrect. Heating is caused by both absorption of SW and LW radiation. It seems odd that the authors only consider the latter (at least this is the impression they give). Also the LW heating rates can be positive (heating) or negative (cooling) depending on the aerosol and temperature vertical profiles whereas the authors seem to associate the interactions of aerosols with LW radiation to a systematic heating of the stratosphere. Please clarify.

Our focus in this paper is on the relative differences between heating rates in the tropical lower stratosphere, where other authors (see Heckendorn et al., 2009) have highlighted the possibility of aerosol heating from geoengineering increasing the stratospheric water vapor concentration. While cooling may result from increasing aerosol concentrations at high latitudes (see Ferraro et al., 2011), heating is the result in the tropical lower stratosphere for the aerosols considered here. We have narrowed our discussion in the paper to apply only to the tropical lower stratosphere, and now consider both LW and SW radiation. And we provide the fractional contribution of SW heating to the total heating: "Shortwave heating from alumina is about 15% of the total heating, and from sulfate about 20%. The total heating rate from diamond is almost entirely due to shortwave effects, but is still much less than that for alumina with the same top-of-atmosphere shortwave radiative forcing."

There are a number of notations and units that need to be clarified (as discussed below).

**Specific comments:**

Page 11800, line 12: sentence is a little unclear (maybe "yet" should read "although") Page 11801, line 5: The study of Ferraro et al (GRL, 2011) could be cited here.

done

Page 11802, line 7: and also "cirrus formation" if the dynamical effects propagate in the upper troposphere as some models suggest.

Cirrus effects are too uncertain (both in sign and in magnitude) for specific mention in our introduction, though we did add the italicized words "these risks include, *but are not limited to*," in that paragraph. Potential cirrus effects are dealt with in section 4.1 under "missing feedbacks".

Page 11802, line 11: a citation to Mercado et al (Nature, 2009) or an earlier paper would seem more appropriate here.

Mercado reference added.

Page 11806, line 3: I am sure the explanation is somewhere in the cited literature, but could you explain why mass is proportional to $R^{D_f}$. A diagram might help to understand.

The relationship between $R_g$ and $N_i$ is found to be a statistical scaling law that holds true over a wide range of $R_0$ and $N_i$ values, with $D_f$ remaining constant for a given material. This relationship is probably related to the coagulation process. Since $N_i$ is proportional to $R_g^{Df}$, and total agglomerate mass is just the mass of a monomer times $N_i$, agglomerate mass is proportional to $R_g^{Df}$. We have modified text as follows:

"Larger particles produced by coagulation assume fractal structures that obey a statistical scaling law where the fractal dimension $D_f$ determines how the size of an aggregate of particles is related to the number of primary particles. … Thus particle mass is proportional to $R_g^{Df}$. The fractal dimension $D_f$ for a given material has been found to be invariant for a wide range of $R_0$ and $N_i$

values."

Page 11807, line 9: what is R? it has not be defined previously. Or do you mean $R_g$?

Changed this R to $R_p$ as it referred to spherical sulfate particles.

Page 11807, line 10: is N the same as $N_i$ defined previously?

Changed N to $N_i$.

Page 11807, line 11: are you talking about area or surface area projection (as on line 3) here? What is area relevant here?

Surface area projection. Text clarified.

Page 11807: I do not pretend I understand the details of fractal aerosols very well, so it would be useful if the authors point to limitations in their model.

Section 4.1 "Geometry of aggregates, effects of size binning" covers these limitations. We added a paragraph about the effects of size binning.

Page 11810, lines 20-30: does this depend on $N_i$?

Yes, sedimentation rates depend on $N_i$. That should be clear from Figure 1 and from the equations for sedimentation rate given in Section 2. We have made no change in text.

Page 11813: I am not sure what the authors mean when they say "fractals never contain more than X monomers''. Surely there must be but in (very) low concentrations?

Modified this discussion to refer to "significant concentrations".

Page 11816, line 5: the word "significant" is used in a very subjective way here. What is a significant or insignificant amount of diffuse radiation for terrestrial ecosystems?

We have rewritten this sentence as: "Thus in geoengineering applications, alumina and diamond would scatter radiation back and produce substantially

smaller increases in diffuse radiation at the surface than would sulfate particles producing the same change in RF."

Page 11816, line 19: scattering becomes negligible per unit mass particle, but not per unit particle. Eventually it depends how much of the mass is in this range of monomers.

We changed the text to read "An aggregate of 16 alumina monomers has negligible scattering per unit mass."

Page 11816, lines 27-29: you should say this earlier.

Moved this sentence into the previous paragraph.

Page 11818, lines 8-9: note that IR radiative effects result in both heating / cooling depending on the altitude and aerosol vertical profile considered.

Our focus in this paper is on the relative differences between heating rates in the tropical lower stratosphere, where other authors (see Heckendorn et al., 2009) have highlighted the possibility of aerosol heating from geoengineering increasing the stratospheric water vapor concentration. Present-day trace gas profiles for the tropics based on reanalysis data are used for our heating rate estimations, along with a uniform aerosol layer between 18 and 23 km in the tropics. While cooling may result from increasing aerosol concentrations at high latitudes (see Ferraro et al., 2011), heating is the result in the tropical lower stratosphere for the aerosols considered here. We have narrowed our discussion in the paper to apply only to the tropical lower stratosphere. We replace "longwave, or infrared (IR), heating in the stratosphere" with "aerosol heating of the tropical lower stratosphere", as we now include both longwave and shortwave heating in our estimates. We add a reference here to Heckendorn et al. (2009) who determined that the heating of the lower stratosphere was primarily caused by IR effects for sulfate. And we later quantify the contributions of LW and SW heating to our totals.

"Aerosol heating of the tropical lower stratosphere is another potential risk of geoengineering. Heckendorn et al. (2009) investigated this effect and the resulting increase in stratospheric water vapor, primarily caused by longwave heating, for sulfate aerosol. … Shortwave heating from alumina is about 15% of the total heating, and from sulfate about 20%. The total heating rate from diamond is almost entirely due to shortwave effects, but is still much less than that for alumina with the same top-of-atmosphere shortwave radiative forcing."

Pages 11816, 11817 and 11818, line 24: are these $Wm^{-2}$ of net (SW+LW) forcing or SW forcing only?

Shortwave only. We have clarified this in the text.

Page 11840: change "mixing ratio" to "mass mixing ratio" for clarity on panels a) and b). A mixing ratio is not the same as a concentration, so the caption should say "Mass mixing ratio" and not a "Concentration in ppbm" !

This has been changed in the Figure 2 caption and figure labels, and on page 11812.

Page 11844, figure 6: I do not understand what is plotted here as the terms used as different from what I am used to. A cross-section is not dimensionless. Is panel (a) showing an upscatter fraction (but the values appear too large)? Or an upscatter cross-section (define) per unit geometrical cross-section? Likewise I am not sure what an upscatter cross-section per unit volume is. This time, it seems the cross-section is not dimensionless as the unit is $\mu m^{-1}$.

The text now reads "Panel (a) shows the upscatter cross-section divided by the geometric cross-section (a dimensionless ratio). Panel (b) shows the upscatter cross-section divided by the particle volume (units of μm-1)…".

## Response to Anonymous Referee #2

First we would like to thank the reviewer for a careful reading of our manuscript and many constructive comments that have improved the quality and clarity of the paper. We have added a table to list the model experiments described and an appendix to detail the coagulation and condensation schemes. We added a paragraph on the limitations and inherent size broadening of a discrete sectional bin scheme. We have included a more thorough description of the AER 2-D model's dynamical fields and PSC parameterization and discuss some model comparisons with observations for both aerosols and ozone. We adjusted our RF values in Figures 7 and 13 due to a correction in the RF albedo adjustment. We added a comparison of ozone change from sulfate geoengineering to that from alumina and diamond geoengineering in Figure 12a. We also replace the unit megatons with terragrams throughout the manuscript. We have added seventeen new references and increased font size and readability of the figures. J. A. Dykema has been added as a co-author (previously recognized in a footnote and acknowledgement) due to his scientific contributions in addressing reviewer questions regarding heating rates and radiative forcing.

Our answers to the reviewer's questions and comments are detailed below, with the reviewer's comments in black and our responses indented and in green.

The manuscript describes a novel approach to manipulate the stratospheric albedo to counteract global warming (geoengineering; solar radiation management, SRM) by releasing solid alumina particles into the lower stratosphere. The authors investigate the response of a two-dimensional coupled aerosol microphysics-stratospheric chemistry model to estimate the desired aerosol radiative forcing and attempt to quantify associated risks concerning the potential increase in diffuse light and impacts on the stratospheric ozone budget.

This study is a necessary step towards a better understanding of this particular research topic. The manuscript is generally well written. Although investigating a new type of aerosol in the (higher) atmosphere, the author's succeed in

introducing the necessary background information without overstraining the reader. Methods are explained fairly good, the quality of figures are matching standards of a scientific journal, and the results seem plausible.

I do have, however, a few concerns which should be addressed before the manuscript is published in ACP.

**General comments:**

The current structure of the paper does not allow to get a quick overview about the experiments which have been conducted and are described, before one has read the entire Sect. 3. Even then it remains unclear, because on several places the author's phrases like „..we perform additional model calculations...", or „... model...for a number of parametric...scenarios...", and so on. The paper would substantially gain in quality if the experiments are briefly described en bloc before the results (even the test cases) are addressed. I suggest to introduce such a (sub-)section before the section „Model results", potentially also including an additional table presenting an overview of what has been tested and which parameter have been adjusted (in my understanding a common practice in manuscripts presenting numerical studies).

> We have added Table 1 to provide an overview of the experiments. We added a new paragraph at end of section 3.1 to reference the table and describe the 10-year model spinup and averaging period.

In this respect I also found it difficult to understand when the model was interactively coupled to a chemistry scheme and when not. Since chemistry is such an important issue for the study, and the author's relatively often emphasize that they assess potential risks associated with the method, I suggest to rephrase respective parts of the manuscript and make chemistry coupling more transparent.

> We'd initially done all the alumina calculation without full chemistry to get burdens and distributions of alumina, then repeated them with full chemistry and aerosols coupled to get the ozone response, which led to the confusion. We have modified the paper to only discuss the results with full interactive chemistry and aerosols so as to avoid confusion. Results are identical except for somewhat different OH concentrations affecting sulfate, which is evident in Figure 9. We've modified the first 2 paragraphs of Section 2 accordingly.

Concerning simulated ozone changes, I wonder why the experiments are not compared in more detail to recent studies investigating ozone changes due to

proposed geoengineering scenarios using SO2 or sulfate (e.g. Tilmes et al. 2008,2009; GeoMIP)? This is a clear deficit of the manuscript. I understand that the model applied here is technically different from other models which have been used to study the geoengineered sulfate-ozone relationship. But I in my understanding of the research topic and chemistry/climate/transport/ aerosol models, several aspects could be elaborated here.

The focus of this paper is on the microphysics of solid aerosols and on a comparative study of the ozone loss from different solid aerosols. A detailed comparison of ozone loss calculations for sulfate aerosol is far beyond this paper's scope. Nevertheless, we do cite the Tilmes references and Pitari et al. (2014) (for GeoMIP studies) and Heckendorn et al. (2009). Unforturnately, none of these studies yield direct comparisons because (1) the emission region is different (others inject at the equator only rather than 30S-30N, and at different altitudes), (2) chlorine and bromine levels are often different, (3) some contain dynamical feedbacks and some don't. However, when we run our model to match the Heckendorn results as closely as possible (narrowing the emission region and eliminating VSL bromine species), we obtain similar values of global ozone change (-4.5% vs -4.75% for 5 Tg-S/yr injections), lending confidence to our calculated ozone changes. Compared to Tilmes, our calculated ozone changes appear to be substantially larger, which may be related to dynamical responses in the WACCM model in the tropics. We have added a sentence to this effect: "Our simulations of ozone change due to $SO_2$ injections are similar to those of Heckendorn et al. (2009) if we compare equivalent scenarios, but larger than those of Tilmes et al. (2012)."

I also would like to see improvements towards are better discussion of aspects related to atmospheric dynamics. For instance, seasonal dependence of results, temperature dependent effects. Both are associated with the underlying meteorology (which is also unclear, see specific comments below). The author's are mentioning phenomena like QBO only briefly when the methodology is described, but never refer to them later when the results are analysed and discussed. An important part of the manuscript deals with stratospheric chemistry, which is known to be temperature dependent, but respective investigations or discussions about e.g. additional errors induced by associated impacts are not considered so far. I think it is recommended to consider such aspects in the revised manuscript.

The purpose of this paper is to present a first look at geoengineering by solid particles, accounting for particle interactions in the stratosphere, and comparing efficacy of different particle compositions and injected monomer

diameters. Aspects such as induced modifications in stratospheric temperature and dynamics await a future study with a coupled chemistry-aerosol-climate model. We discuss these limitations in Section 4.1. The dynamical fields used in our model study are now described in more detail in Section 2. We have added one sentence to Section 4.1, *Missing Feedbacks*: "However, Heckendorn et al. (2009) found that ozone loss due to heterogeneous chemistry, without the dynamical effects of changes in temperature, water vapor, and the Brewer-Dobson strength, accounted for 75% of the ozone change." which demonstrates that our study, while not perfect, is still quite useful.

With respect to diamond aerosols proposed as a forcing agent, I do not really understood the message of respective parts of the study. Does the manuscript really profits from the diamond aspects? In opinion not - instead the additionally considered diamond investigations lead to some confusion because the subject is discussed only here and there in the manuscript, only a few figures, for instance, contain data from the diamond simulations and so on. I suggest to critically examine whether it is really helpful to investigate this additional compound here.

Diamond is an example of a class of high-index compounds (e.g., zirconia, SiC silicon carbide) that, due to more favorable upscatter to forward scatter ratios, *might* enable solar geoengineering with lower side effects than sulfate aerosol so we think it's important to keep the analysis of diamond in the paper. Table 1 helps to clarify which calculations we have performed for diamond. Diamond is omitted from some figures because the results are so close to alumina at 160 nm that it would clutter the figures for no reason. We do state that diamond results are not shown but similar to alumina at 160 nm for Figure 1 (sedimentation velocities) and Figure 5 (burdens), and added similar statements for Figures 3 and Figure 10.

**Specific comments:**

Please include a list of abbreviations (e.g. MSA, QBO, ...).

We have spelled out abbreviations (MSA, DMS, QBO, PSC) where they are used.

p11801 lines 14-23: Is it a chemistry coupled model ? should be mentioned here.

Yes. We have added a sentence to this paragraph: "The chemistry and aerosol schemes in the model are interactive, while dynamical fields are prescribed."

p11802 lines 2ff: The author's attest "other" models a good job in quantifying the

response to idealized SRM methods - which in my opinion is too speculative since such idealized scenarios cannot be proved in reality, so that a less subjective valuation seems appropriate here.

Given that Kravitz et al. (2014) have now repeated the results in Moreno-Cruz et al. (2011) using the entire CMIP-5 ensemble we stand by our claim of these results are both surprising and representative of the current universe of climate models used for climate science and policy. We have modified the wording of this statement to clarify that it applies to model-simulated climate changes: "Results from a large set of climate models suggest that idealized SRM can do a surprisingly good job in reducing model-simulated climate changes, both locally and globally, which, in our view, is a primary motivation for continued research on SRM (Kravitz et al., 2014; Moreno-Cruz et al., 2011)."

p11805 lines 1-4: Since also in a 2-D model the dispersion of aerosols, hence the desired aerosol effect, depend on the transport characteristics of the model, please describe in more detail the underlying methodology referring to Fleming et al (1999).

We modified the discussion of the model's transport as follows: "The model's 2-D transport is prescribed based on calculations by Fleming et al. (1999) for each year from 1978 to 2004, employing observed temperature, ozone, water vapor, zonal wind, and planetary waves. Different phases of the quasi-biennial oscillation (QBO) are included in the observational data employed. We average the transport fields over the years 1978-2004 into a climatology and employ that circulation each year of our ten year calculations."

p11805 line 11: In my understanding it was not the goal of the SPARC Assessment of Stratospheric Aerosol Properties (ASAP, 2006) to rate participating models or to introduce any kind of metric for them, I strongly suggest to chose a less qualitative statement instead of „best".

We have removed the quantitative model rating attributed to SPARC (2006) and now include a few sentences describing model comparisons to observations, including mention of model deficiencies.

p11805 line 12: The understanding of mechanisms forming new aerosols in the stratosphere is far from being clear so that I suggest to rephrase the sentence, e.g. using a formulation like „is thought to form by" or „may nucleate".

Changed wording: "Sulfate aerosol formation is thought to be initiated mainly by binary homogeneous nucleation of $H_2SO_4$ and $H_2O$ vapors, primarily in the tropical tropopause region."

p11805 lines 18-20: Logarithmically spaced bins?

Modified to read: "The model uses a sectional representation of particle sizes, with 40 logarithmically-spaced sulfate aerosol bins, representing sizes from 0.39 nm to 3.2 μm, with aerosol volume doubled between adjacent bins."

p11805 line 20: You are referring to sedimentation and wet deposition here, but only the former is described below. Please make a note that a description of sedimentation follows and add (at least) references describing how wet deposition is handled in the model.

Added: "The sedimentation formulation is described below. Rainout/washout process are represent by a first order loss term in the troposphere with removal lifetime ranging from 5 days at the surface to 30 days at the tropopause."

p11806 lines 5-10: Please add references to the two equations.

We moved the Filippov and Maricq references to before the equations for clarity.

p11803/4 and Sect. 3.1: The description of the use of diamond with respect to "the primary test case" is confusing. When I interpret the figures correctly, the authors show results from a "diamond simulation" only in the 6th Figure (and later), but describe the compound and related experiments at the beginning of the results section. Again, an experiment table would help to clarify this issue.

We added Table 1 to list the numerical experiments performed. Diamond is omitted from some figures because the results are so similar to alumina at 160 nm (density difference is the only difference affecting aerosol distribution and mass in our simulations) that it would clutter the figures for no reason. We do state that diamond results are not shown but similar to alumina at 160 nm for Figure 1 (Sedimentation velocities) and Figure 5 (burden). We added similar statements to the discussion of Figure 3 showing the size distributions and Figure 10 showing surface area density.

Sect.3.2 and Sect. 3.3: Until the first results are described about the Figures 1 & 2, I do not find any information about the integration period of the model. When did you start the model, how long was it integrated and so on. This is a clear deficit of the manuscript and should be corrected. Please describe in detail the settings but also mention which averaging period has been used for the figures, otherwise the results are meaningless (some figures do contain this information, but some do not).

We added to the end of section 3.1: "Each scenario is calculated with a 10 year integration period, using dynamical fields representing the 1978-2004 average repeated each year and fixed boundary conditions from approximately the year 2000, until an annually-repeating result is

achieved. We analyze results from the final year of each calculation, concentrating on annual average conditions."

p11810 referring to Fig.1: As above, for which period of integration? Shown for steady state, annual mean? Is the latitude band the same as for the upwelling?

The original plotted sedimentation velocities were for April at 28N. These velocities are not very sensitive to latitude or season. For consistency with the tropical upwelling velocities, we now present annual averages from 20S-20N for aerosol sedimentation velocities. We added this information to the text and the figure caption.

p11811 lines 9-11: In terms of mass or mixing ratio?

Most stratospheric sulfate exists in condensed form in terms of mass. The word "mass" has been added.

p11812 lines 6-7: Does it mean you performed a spinup over 10 years and then started to analyse the results? I assume with emissions you refer to surface and/or volcanic emissions (of S compounds).

Yes, we do a spinup for 10 years and ignore the transient response, reporting the steady-state response, which does not change from year-to-year thereafter. Emissions referred to the stratospheric injection of particles for geoengineering. We have changed "emission" to "injection" here and in many other places in the manuscript to avoid confusion. This sentence now reads "Stratospheric particle injections are continuous in time…"

p11812 lines 21ff & Fig.2 a,b: The top panel show mixing ratios but in the paragraph the authors infer and compare the burden from the figures. In my understanding the burden is a vertically integrated quantity which is not easy to infer (visually) from a concentration altitude-latitude plot. In particular not, when the legends of the plots are different. Please adjust and/or calculate/plot the burden.

By burden, we refer to integrated stratospheric burden which is shown in Figure 5. We have eliminated the discussion of burden in reference to Figure 2 to avoid confusion and instead discuss peak mass mixing ratio.

p11813 lines 22ff & Fig. 4: When I understand it correctly, the green curves should resemble the values of the bars of Fig. 3 b-d? Mentioning that in the paragraph would help to better understand the result.

Yes. We added the sentence: "The 1 Tg $yr^{-1}$ cases (green lines) match the global

mass fractions shown in Figure 3."

p11814 lines 22ff & Fig. 5b: Do you also show here sulfate from Pierce et al (2010) as in panel a? I think not - the caption is a little confusing for me. Also the beginning of the paragraph is a bit misleading, as it indicates that you are showing sulfate here (only). I suggest to introduce the burden issue with a statement about alumina in order to avoid confusion. I am also not sure why the sulfate burden increases - I thought you emit sulfur continuously (assuming it continuously reaches the stratosphere) so that the sulfur content of the stratosphere is an equilibrium state (you model quasi a background Junge layer). Then I would assume to find a constant sulfate burden in the model (assuming this is an annual mean). Or is it because I cannot distinguish thick lines from thin lines?

No, panel (b) does not include simulations of $SO_2$ or $H_2SO_4$ geoengineering injection, as those increase sulfate burden by many times above the background level and would require a different plotting scale. The sulfate lines that increase continuously from 1 Tg/yr to 8 Tg/yr are the thin lines representing sulfate fraction on alumina particles. The thick lines contain circles and the thin lines don't (noted in caption) and there are arrows in the figure pointing to the respective y-axes to help distinguish them. The paragraph starting on line 22 of page 11814 refers to Figure 5(b) only, so discusses only sulfate burden. We clarified by stating that the scenarios presented in this figure refer to geoengineering injection of alumina and that the sulfate burdens are shown as a function of the geoengineering injection rate of alumina. Sulfate burden changes as a function of alumina injection because the sulfur coating the alumina particles sediments faster than pure sulfate particles would in most cases.

p11815 line 16/17: Please add references in order to make clear how you calculated the upscatter cross section. Same for the other parameter panel in Fig. 6 b,c.

We now include the following description and references: "We calculated the solid particle monodisperse single scatter albedo values from Mie Theory (Bohren and Huffman 2008) using tabulated complex refractive index data for diamond (Edwards and Philipp 1985) and alumina (Thomas and Tropf 1997). The upscatter and downscatter cross sections are calculated from Wiscombe and Grams (1976), utilizing the scattering phase function from Mie Theory and the same complex refractive index data."

p11816 line 7ff & Fig. 7: Again, what is the time period you are showing? Shortwave, cloud-free forcing only?

Time period is annual average of steady-state result. RF is for shortwave

only under cloud-free conditions. We now specify "global annual average top-of-atmosphere shortwave radiative forcing … under clear sky conditions."

p11817 lines 21-24: Is there any possibility to estimate the uncertainty you mention? Wouldn't it be possible to estimate upper and lower bounds of associated errors, at least for the most „promising" scenario only?

The error in these calculations is about 20% when compared to a more complete RT model for the same physical assumptions. As our objective is to obtain well-founded estimates of radiative forcing for comparison with sulfate geoengineering, and relative efficiencies among solid particle scenarios, an estimate of associated errors is outside the scope of this paper. However, John Dykema of our group is preparing a detailed radiative study with RRTM to address this complex topic in a future paper.

p11818 lines 2-7: Two things are not clear:

a) I am a little confused about "per megaton". In Fig 7a it refers to "per megaton burden" - which is different to Fig 7b where it refers to "per megaton injection"?

Correct. The units on the y-axis of Figure 7a are watt per $m^2$ per Tg of atmospheric burden. We use this quantity to scale the atmospheric burden for each aerosol bin (bins shown in the x-axis of Figure 7a as "# cores in particle") and sum over bin sizes for each scenario to obtain Figure 7b.

b) About sulfate, lines 4-7: I though that is what you show. What is the methodology of H2SO4 (and SO2) in Fig. 7b if not direct injection? And, if different from Fig. 5, please make it clear.

Perhaps the confusion here is using the words "injection" and "emission" to both refer to geoengineering injections directly into the stratosphere. We have have replaced "emission" with "injection" to try and avoid this confusion.

p11818 lines 8-25: LW effects are estimated offline from your results with the AER model? do you show data for one year only in Fig. 8?

Correct that radiative effects are estimated offline. Our heating estimates use the annual average particle number densities in the tropical lower stratosphere from the AER model over the last year of simulation when steady-state has been reached. Figure 8 shows an annual average over the final year of simulation as well.

p11819 line 15: What context for “preliminary“?

Simply that, as this is our first paper on this topic, we have focused on the aerosol microphysics and on an investigation of the comparative ozone loss between different particle injection scenarios. A more complete study of ozone loss would require better characterization of some of the surface reaction coefficients, and this requires new laboratory studies. More detailed modeling would also require a sophisticated radiative transfer model coupled to a chemistry-climate-aerosol model and would utilize future Cl and Br abundances.

p11819 lines 16-18: I do not understand the whole sentence „To enable comparison of the ozone impact of sulfate geoengineering we use the same model to compute change in ozone abundance arising from injections of both solid particles and of sulfate aerosols.“. What do you mean with „the same model“?

We don’t plot results from Pierce et al. or Heckendorn et al., but have repeated their calculations to be consistent with others in this paper. The injection method is the same as Pierce et al. (injection 30S-30N, 20-25 km) though that work did not show ozone changes. Heckendorn et al. showed ozone changes, but for injections at the equator and 20 km only, and from a 3-D coupled chemistry-climate model. Table 1 should clarify this. We have added the word “relative” in “To enable a relative comparison of the ozone impact of sulfate geoengineering…”

p11819 lines 18ff: Are there any references available for the coupled aerosol-chemistry AER model? E.g. studies showing the capability of the coupled model to simulate certain characteristics of the stratospheric chemistry system - characteristics/features which are well known and explored by a range of other studies? Please add. If such references does not exist, I suggest to include a complete table of reactions, potentially as supplementary material, in order make the respective information available for the reader.In the same paragraph, please add also references for the methodology concerning the treatment of PSCs and the underlying meteorological climatology as well (see comments made earlier).

We added four references regarding the AER model: Rinsland et al. (2003), Weisenstein et al (1998; 2004), and Anderson et al. (2006), of which only the Weisenstein et al. (1998) reference employed aerosol-chemistry coupling, while the other include details of the chemistry scheme and gas-phase comparisons with observations. We also added the sentence: “A comparison with observed ozone trends between 1979 and 2000 is presented in Anderson et al. (2006) for the AER model and several other models.”

The transport and temperature climatologies are covered earlier in Section 2. We added references and more detail to our description of PSC treatment: “The model parameterizes polar stratospheric clouds (PSCs) using thermodynamic equilibrium, employing the formulas of

Hanson and Mauersberger (1998) and Marti and Mauersberger (1993) for equilibrium vapor pressures over solid $HNO_3$ and ice, respectively, assuming no supersaturation and prescribing the particle radii." But our results do not depend on the PSC treatment, as the polar regions represents only 13% of the global atmospheric mass, with PSCs present only seasonally. Reactions on liquid sulfate aerosols, including in the polar regions, are much more important globally.

p11820 line 4: Please add „primarily" before „Cl".

done

p11820 line 4ff: Please make clear that you refer to future conditions. In the context of the ozone Section 3.5, you refer to „present day conditions" - how does the time period(s) match with your emission scenarios of S compounds?

We changed this sentence to read: "Future concentrations of halogens are expected to decline…" We use present day concentrations of sulfur compounds as well as chlorine/bromine, $N_2O$, etc. for this study. Our discussion of Table 1 in Section 3.1 states that "fixed boundary conditions from approximately the year 2000" are used.

p11821 line 5-7, Fig. 9 b, c: The response of the 80 nm alumina injection is very different from that of 240 nm. To me it suggests that in the 80 nm case sulfate is more rapidly dispersed towards the poles as in the 240 nm case. Do you have any idea why the behavior is so much different, e.g. from a dynamical perspective?

The difference in sulfate surface area density between the 80 nm and 240 nm alumina cases is due to (a) the faster sedimentation of 240 nm monomers compared to 80 nm monomers, which results in strongly decreasing concentrations of alumina away from the tropical injection region with 240 nm monomers injected (see Figure 2), and to (b) the large $R_g$ of the complex fractal structures composed of 80 nm monomers which efficiently scavenge the smaller sulfate particles. We added the following to the paper: "With injection of 80 nm monomers, the sulfate SAD has increased by factors of 2-4 in the lower stratosphere, with maximum SAD at high latitudes where significant concentration of complex alumina fractals exist to scavenge the smaller sulfate particles. With injection of 240 nm monomers, the maximum sulfate SAD occurs in the tropics as the faster sedimentation of alumina in this case results in a smaller concentration of mostly monomers at high latitudes."

p11821 line 13-14:I do not understand the sentence „We would expect similar chemical ozone loss from similar changes in sulfate SAD whether due to geoengineering by $SO_2$, $H_2SO_4$, or alumina injection." In a general context?

We have clarified by modifying this sentence to read: "For reactions that are dominated by liquid sulfate surface area density, we would expect similar chemical ozone loss from similar changes in sulfate SAD whether due to geoengineering by $SO_2$, $H_2SO_4$, or alumina injection."

p11821 line 25:Please add „uncoated" before „alumina SAD".

done

p11823 line 14:You are mentioning the „transport timescale“. For me it is even unclear what the timescale at all is, concerning simulation period, meteorology, analysis.

We refer here to local balances between chemical production, destruction, and transport rates that determine ozone concentrations in different regions of the atmosphere. We have modified this to read: “The annual average ozone change as a function of latitude and altitude (Fig. 11, right hand panels) shows features linked to local balances in ozone’s formation rate, chemical destruction rate, and local transport rates.” We then explain for the tropics and midlatitude middle and lower stratosphere which ozone tendency terms are most important.

p11828 lines 9-15:Does it mean the aerosol scheme is not interactively coupled to the transport model’s radiation scheme? If so, please make it clear here and in Sect. 2 and describe briefly how heating rates are handled in the model (prescribed?) and how this relates to the transport of aerosols.

Yes, the radiation and aerosol schemes are uncoupled. The transport and temperature fields are described in more detail now in Section 2. Here we have added: “The modeling we present utilizes temperature and transport fields uncoupled from the model’s chemistry and aerosols and is therefore missing a number of feedback processes that may be important…” We also provide a quantitative estimate of the importance of these feedbacks: “However, Heckendorn et al. (2009) found that ozone loss due to heterogeneous chemistry, without the dynamical effects of changes in temperature, water vapor, and the Brewer-Dobson strength, accounted for 75% of the ozone change.”

p11829 paragraph 2 (also affecting other sub-sections of Sect. 4):It would be helpful to insert cross references to the figures here in order to make it easier to understand what you mean, and to make it possible for the reader to find the features you discuss in the figures. In particular, I have difficulties to approve the last sentence of paragraph 2, which sounds contradictory at a first glance.

We have added these cross-references. Thank you for the excellent suggestion.

p11829 line 28-29:Please remind the reader that the ozone changes depend on specific model assumptions, e.g. add „under the assumptions made“ or so.

Modified the sentence to read: “The annual global average ozone column is reduced by 3.6% with maximum ozone loss of 4 to 7% over polar regions for this scenario and the given modeling assumptions.”

p11830 lines 8ff:Difficult to interpret. When you switch off reaction R1 or switch off the coating, to which injection scenario or alumina sizes do you refer with the calculated changes in %?

Injection of 4 MT/yr alumina of 240 nm monomer radius. This has been clarifed in the text.

**Technical comments about figures:**

Please increase the readability of numbers and indices in the figures 1,2, 4, 5, 7, 8 - 13. I would like to see the line plots Fig. 1, 4, 5, 7, 10, 12 (!!), and 13 enlarged.

We have enlarged the numbers and labels on all the plots except for Fig 3.

Figure 6: Please use a different color for the magenta curves (on poor resolving printer they may be indistinguishable from reddish colors).

We have replaced the magenta lines with another color except where the colors are also distinguished by symbols.

Figure 9: If appropriate, please use decimal numbers for the legend in panel a. To better differentiate the contour plot in panel a from the deviations/differences shown in panels b-d, I suggest to use a different colorbar for the the latter, e.g. a gradient turning from blueish (for negative values) to reddish (for positive values) colors, with a transition around zero marked in white or very bright colors (alternatively use a contour line to mark zeros).

The colorbar labels in panel (a) are now decimal numbers. Most of the negative values in panels (b-d) were eliminated when we used a more consistent baseline (from the interactive chemistry-aerosol model) to get differences.

Figure 11: I see a similar same colorbar issue as for Fig. 9.

We have not changed the colorbars in Fig. 9.

# Author response to Interactive Comment by M. J. Tang
28 July 2015

Interactive comment on
"Solar geoengineering using solid aerosol in the stratosphere"
by D. K. Weisenstein and D. W. Keith

M. J. Tang mingjintang@gmail.com

Received and published: 28 April 2015

This study is quite novel and interesting for the SRM research community. Congratulations.

In the manuscript it is stated that important reactions on the surface of these solid SRM particles are not studied. May I bring your attention to the laboratory measurements funded by the UK SPICE project? We have investigated the heterogeneous reactions of these SRM particles (mainly $TiO_2$, but also $SiO_2$ and other solid particles) with $N_2O_5$, $ClONO_2$, and $O_3$.

The work on $N_2O_5$ was published recently (Tang et al., 2014a; Tang et al., 2014b), and the effect of heterogeneous reactions of $N_2O_5$ with $TiO_2$ particles on ozone was also assessed using a 3-D global model (Tang et al., 2014a). Our work on $ClONO_2$ and $O_3$ will be submitted soon.

Reference:

Tang, M. J., Telford, P. J., Pope, F. D., Rkiouak, L., Abraham, N. L., Archibald, A. T., Braesicke, P., Pyle, J. A., McGregor, J., Watson, I. M., Cox, R. A., and Kalberer, M.: Heterogeneous reaction of $N_2O_5$ with airborne $TiO_2$ particles and its implication for stratospheric particle injection, Atmos. Chem. Phys., 14, 6035-6048, 2014a.

Tang, M. J., Camp, J. C. J., Rkiouak, L., McGregor, J., Watson, I. M., Cox, R. A., Kalberer, M., Ward, A. D., and Pope, F. D.: Heterogeneous Interaction of SiO2 with $N_2O_5$: Aerosol Flow Tube and Single Particle Optical Levitation-Raman Spectroscopy Studies, J. Phys. Chem. A, 118, 8817-8827, 2014.

Interactive comment on Atmos. Chem. Phys. Discuss., 15, 11799, 2015.

We thank M. J. Tang for reading and commenting on our manuscript. We are aware of the works mentioned and appreciate their significance. Because these studies are not directly applicable, as neither alumina nor diamond were tested, we did not cite them in the initial manuscript. However, they are applicable to the topic in general and a valuable reference in this developing field, so we have added a citation to these studies in the introduction. And we replaced the statement that "rates of important chemical reactions remain unmeasured" with "the rates of many potentially important chemical reactions remain unmeasured".

Now the 7th paragraph of the introduction reads, in part:

"The use of solid aerosols, however, introduces new risks that require evaluation. The dry surfaces of the solid aerosols, for example, may catalyze reactions that cause ozone loss (Tang et al., 2014a; 2014b). This risk is hard to evaluate because the rates of many potentially important chemical reactions remain unmeasured for substances such as diamond that are novel in the stratosphere."

# Solar geoengineering using solid aerosol in the stratosphere

**D. K. Weisenstein[1], D. W. Keith[1,2], and J. A. Dykema[1]**

[1]School of Engineering and Applied Science, Harvard University, Cambridge, MA, USA

[2]Kennedy School of Government, Harvard University, Cambridge, MA, USA

Correspondence to: D. K. Weisenstein (dkweis@seas.harvard.edu)

## Abstract

Solid aerosol particles have long been proposed as an alternative to sulfate aerosols for solar geoengineering. Any solid aerosol introduced into the stratosphere would be subject to coagulation with itself, producing fractal aggregates, and with the natural sulfate aerosol, producing liquid-coated solids. Solid aerosols that are coated with sulfate and/or have formed aggregates may have very different scattering properties and chemical behavior than do uncoated non-aggregated monomers. We use a two-dimensional chemistry-transport-aerosol model to capture the dynamics of interacting solid and liquid aerosols in the stratosphere. As an example, we apply the model to the possible use of alumina and diamond particles for solar geoengineering. For 240 nm radius alumina particles, for example, an injection rate of 4 Tg yr$^{-1}$ produces a global-average shortwave radiative forcing of 1.2 W m$^{-2}$ and minimal self-coagulation of alumina although almost all alumina outside the tropics is coated with sulfate. For the same radiative forcing, these solid aerosols can produce less ozone loss, less stratospheric heating, and less forward scattering than do sulfate aerosols. Our results suggest that appropriately sized alumina, diamond or similar high-index particles may have less severe technology-specific risks than do sulfate aerosols. These results, particularly the ozone response, are subject to large uncertainties due the limited data on the rate constants of reactions on the dry surfaces.

## 1 Introduction

Debra Weisenstein 8/25/2015 9:08 AM
**Deleted:** and

Debra Weisenstein 7/9/2015 11:08 AM
**Deleted:** chemical transport

Debra Weisenstein 7/21/2015 12:48 PM
**Deleted:** Mt yr

Debra Weisenstein 8/12/2015 4:55 PM
**Deleted:** 3

Debra Weisenstein 5/27/2015 9:42 AM
**Deleted:** yet

Solar geoengineering, or Solar Radiation Management (SRM) is the possibility of deliberately introducing changes to the Earth's radiative balance to partially offset the radiative forcing of accumulating greenhouse gases and so lessen the risks of climate change. Most research on SRM has concentrated on the possibility of adding aerosols to the stratosphere, and essentially all atmospheric modeling of stratospheric aerosol injection has focused on increasing the loading of aqueous sulfuric acid aerosols (Rasch et al. 2008; Heckendorn et al., 2009; Niemeier et al., 2011; Pitari et al., 2014). The possibility that solid aerosol particles might offer advantages over sulfates, such as improved scattering properties, was first suggested almost two decades ago, but analysis has been almost exclusively limited to conceptual studies or simple radiative transfer models (Teller et al., 1997; Blackstock et al., 2009; Keith, 2010; Ferraro et al., 2011; Pope et al., 2012).

Any solid aerosol injected directly into the stratosphere for geoengineering purposes would be subject to coagulation with itself and with the natural background or volcanic sulfate aerosol. Aggregates of solid aerosols have very different physical structure and scattering properties than do liquid sulfate aerosol particles. The lifetime and scattering properties of a solid aerosol are strongly dependent on these dynamical interactions, and the chemical properties of the aerosol depend on the extent to which it becomes coated by the ambient sulfate.

We have modified the Atmospheric and Environmental Research (AER) two-dimensional chemistry-transport-aerosol model (Weisenstein et al., 2004; 2007) to capture the dynamics of interacting solid and liquid aerosols in the stratosphere. Our model now includes a prognostic size distribution for three categories of aerosols: liquid aerosols, solid aerosols, and liquid-coated solid aerosols. The model's coalescence kernel has been modified and extended to parameterize the interactions of particles across size bins and between all combinations of the three categories. The surface area, sedimentation speed, and coalescence cross-section of an aggregate of solid particles depend on the geometry of the aggregate. The model parameterizes this physics using a fractal dimension and allows that fractal dimension to change with age or with a liquid coating. The chemistry and aerosol schemes in the model are interactive, while dynamical fields are prescribed.

Turning now to the context of this work, it is useful to divide overall consideration of the risks and efficacy of SRM into two components. First, the ability, or *efficacy*, of idealized SRM—

Debra Weisenstein 5/27/2015 9:45 AM
**Deleted:** Pope et al., 2012;

Debra Weisenstein 7/9/2015 11:11 AM
**Deleted:** s

Debra Weisenstein 7/8/2015 4:44 PM
**Deleted:** sulfate

Debra Weisenstein 7/8/2015 4:44 PM
**Deleted:** 1997

conceived as a reduction in the solar constant—to compensate for the risks of accumulating greenhouse gases. And, second, the *technology-specific risks* of any specific engineered intervention that produces a change in radiative forcing. Uncertainty in the efficacy of SRM, the first component, rests on uncertainty in the climate's large-scale response to forcing. Results from a large set of climate models suggest that idealized SRM can do a surprisingly good job in reducing model-simulated climate changes, both locally and globally, which, in our view, is a primary motivation for continued research on SRM (Kravitz et al., 2014; Moreno-Cruz et al., 2011).

Evaluation of the technology-specific risks depends on the specific technology. For sulfate aerosols these risks include, but are not limited to, (a) ozone loss, (b) radiative heating of the lower stratosphere which causes changes in atmospheric temperature and dynamical transport, and (c) the fact that sulfates produce a relatively high ratio of downward scattering to upward scattering so that they substantially increase the ratio of diffuse to direct radiation (Kravitz et al., 2012) which in turn may alter atmospheric chemistry and ecosystem functioning (Mercado et al., 2009; Wilton et al., 2011). In addition to the risks, it may be difficult to produce sufficiently large radiative forcings using $SO_2$ because of the decreasing efficiency at higher $SO_2$ inputs (Heckendorn et al., 2009; English et al., 2012).

The use of solid particles for SRM offers the *potential* to address all of the limitations of sulfate particles. Solid aerosols do not, for example, directly increase the stratospheric volume of the aqueous sulfuric acid that drives hydrolysis reactions, an important pathway through which sulfate aerosols cause ozone loss. In addition, some solid aerosols (e.g., diamond, alumina, or titania) have optical properties that may produce less heating in the lower stratosphere (Ferraro et al., 2011), and any solid with a high index of refraction can reduce forward scattering.

The use of solid aerosols, however, introduces new risks that require evaluation. The dry surfaces of the solid aerosols, for example, may catalyze reactions that cause ozone loss (Tang et al., 2014a; 2014b). This risk is hard to evaluate because the rates of many potentially important chemical reactions remain unmeasured for substances such as diamond that are novel in the stratosphere. Moreover, by spreading the natural background sulfuric acid over a larger surface area as will occur when background sulfate coats the solid particles, the addition of solid aerosols will increase reactions that depend on sulfate surface area density rather than sulfate volume.

Debra Weisenstein 7/26/2015 10:15 PM
**Deleted:** local and global

Debra Weisenstein 5/22/2015 2:41 PM
**Deleted:** ;

Debra Weisenstein 5/22/2015 2:41 PM
**Deleted:** and t

Our motivation for studying solid particles is the possibility that they enable a decrease in the risks of SRM (e.g., ozone loss) or an increase in its efficacy such as the ability to produce larger radiative forcings, or an improved ability to "tune" the spectral or spatial characteristics of the radiative forcing (Blackstock et al., 2009; Keith, 2010). This is in contrast to much of the prior literature that has focused on the potential of solid particles to deliver higher mass-specific scattering efficiency, thus reducing the amount of material needed to produce a given radiative forcing. We do not see this as an important motivation as it appears that the cost of lofting materials to the stratosphere is sufficiently low that cost is not an important barrier to implementation of SRM (McClellan et al., 2012).

In this paper, our focus is on developing the tools and methodology for assessing the risks and performance of solid particles injected into the stratosphere for SRM. The tool described here is a new solid-liquid stratospheric aerosol model, and the methodology is a comparison of environmental side-effects such as ozone loss and forward scattering as a function of the global radiative forcing. We use aluminum oxide (alumina) aerosol as the primary example. Diamond appears to be superior to alumina in several respects, perhaps the most important being that it has minimal absorption in the thermal infrared. We examine diamond, but choose alumina as the primary example because there is a broad basis to examine alumina's potential environmental impacts. Unlike many other solid particles proposed for SRM, there is prior work examining alumina's impacts on stratospheric chemistry (Danilin et al., 2001; Jackman et al., 1998; Ross and Shaeffer, 2014), work that was produced from NASA-funded studies starting in the late 1970's motivated by concerns about the ozone impact of space shuttle launches (alumina is a major component of the shuttle's solid rocket exhaust plume). Moreover, alumina is a common industrial material with a high index of refraction for which there is substantial industrial experience with the production of nanoparticles (Hinklin et al., 2004; Tsuzuki and McCormick, 2004). With respect to potential environmental impacts of alumina deposition on Earth's surface, the fact that aluminum oxides are a common component of natural mineral dust deposition provides a basis for assessing impacts (Lawrence and Neff, 2009). For diamond, there is evidence that diamond nanoparticles are nontoxic to biological systems (Shrand et al., 2007). A much more substantive assessment of the human health and ecosystems impacts of any proposed solid aerosol would be required, however, prior to serious consideration of their use for geoengineering.

The remainder of this paper is organized as follows. The solid-liquid model is presented in Section 2, results for geoengineering injection of alumina and diamond in Section 3, and discussion in Section 4.

## 2 Aerosol model

We have incorporated solid aerosols into the AER 2-D chemistry-transport-aerosol model (Weisenstein et al., 1997; 2004; 2007). The aerosol module, which employs a sectional scheme, has been modified to include three separate classes of aerosols, each with its own size distribution: solid particles, liquid $H_2SO_4$-$H_2O$ particles, and mixed solid-liquid particles. To fully specify the mixed particles we keep track of the volume of liquid $H_2SO_4$-$H_2O$ solution coating the mixed particles. Unlike liquid particles that coagulate into larger spheres, solid particles coagulate into fractal structures with more complex properties. The fractal properties are required to predict the effective size of the particles appropriate to determining coagulation interactions and gravitational settling. Fractal properties are also needed to determine the condensation rate of $H_2SO_4$ gas onto alumina particles and the aerosol surface area density that is important to heterogeneous chemistry and ozone depletion.

The AER 2-D model includes standard chemistry relevant to ozone (Weisenstein et al., 2004) as well as aerosol microphysics and the relevant sulfur chemistry (Weisenstein et al., 1997; 2007). The model includes sulfur-bearing source gases dimethyl sulfide (DMS), $CS_2$, $H_2S$, OCS, and $SO_2$ emitted by industrial and biogenic processes as well as the product gases methyl sulfonic acid (MSA), $SO_2$, $SO_3$, and $H_2SO_4$. Chemical reactions affecting sulfur species are listed in Weisenstein et al. (1997) and their rates have been updated according to Sander et al. (2011). Values of OH and other oxidants are calculated interactively along with ozone and aerosols (Rinsland et al., 2003; Weisenstein et al., 2004). Further description of the chemistry directly relevant to ozone is included in Section 3.5. The model's 2-D transport is prescribed based on calculations by Fleming et al. (1999) for each year from 1978 to 2004, employing observed temperature, ozone, water vapor, zonal wind, and planetary waves. Different phases of the quasi-biennial oscillation (QBO) are included in the observational data employed. We average the transport fields over the years 1978-2004 into a climatology and employ that circulation each year of our ten year calculations. Temperature fields are also prescribed based on climatological



Debra Weisenstein 7/8/2015 4:28 PM
**Deleted:** AER 2-D sulfate aerosol model

Debra Weisenstein 7/20/2015 1:25 PM
**Deleted:**

Debra Weisenstein 7/8/2015 4:29 PM
**Deleted:** ,

Debra Weisenstein 7/8/2015 4:30 PM
**Deleted:** which

Debra Weisenstein 7/8/2015 4:36 PM
**Deleted:** aerosol

Debra Weisenstein 7/8/2015 4:31 PM
**Deleted:** . The

Debra Weisenstein 7/8/2015 4:31 PM
**Deleted:** model has

Debra Weisenstein 7/8/2015 2:57 PM
**Deleted:** which

Debra Weisenstein 7/8/2015 4:13 PM
**Deleted:** base

Debra Weisenstein 7/13/2015 2:48 PM
**Deleted:** t

Debra Weisenstein 7/24/2015 4:12 PM
**Deleted:** (Weisenstein et al., 1997; 2007)

Debra Weisenstein 7/13/2015 2:48 PM
**Deleted:** .

Debra Weisenstein 7/13/2015 2:48 PM
**Deleted:** are chemical products

Debra Weisenstein 7/8/2015 4:17 PM
**Deleted:** taken from previous calculations of the AER 2-D model with full ozone chemistry

Debra Weisenstein 7/8/2015 4:20 PM
**Deleted:** for model runs not requiring ... [1]

Debra Weisenstein 7/20/2015 1:30 PM
**Deleted:** ,

Debra Weisenstein 7/20/2015 1:30 PM
**Deleted:** which

Debra Weisenstein 7/8/2015 4:47 PM
**Deleted:** e

Debra Weisenstein 7/8/2015 4:38 PM
**Deleted:** d

Debra Weisenstein 7/20/2015 1:31 PM
**Deleted:** ,

Debra Weisenstein 7/20/2015 1:31 PM
**Deleted:** and

Debra Weisenstein 7/20/2015 1:31 PM
**Deleted:** ,

Debra Weisenstein 7/20/2015 1:31 PM
**Deleted:** and

Debra Weisenstein 7/20/2015 1:32 PM
**Deleted:** represents a climatological a ... [2]

observations for the same averaging period. The domain is global, from the surface to 60 km, with resolution of 1.2 km in the vertical and 9.5 degrees in latitude. Though the model is primarily suited to modeling the stratosphere and upper troposphere, it does contain a parameterization of tropospheric convection (Dvortsov et al., 1998) that serves to elevate $SO_2$ concentrations in the tropical upper troposphere.

The AER 2-D aerosol model, along with several other 2-D and 3-D models, was evaluated and compared to observations in SPARC (2006). The AER model was found to reasonable represent stratospheric aerosol observations in both nonvolcanic conditions and in the period following the eruption of Mt Pinatubo. Noted deficiencies, common to most models, included too high calculated values of aerosol extinction in the tropics between the tropopause and 25 km as compared to SAGE II extinctions at 0.525 and 1.02 μm during nonvolcanic periods. The growth and decay of the stratospheric aerosol layer following the Mt. Pinatubo eruptions was generally well-represented by the AER model as compared to lidar and satellite observations from 1991 to 1997, though uncertainties in the initial $SO_2$ injection amount and vertical distribution limit our interpretation. Dynamical variability on short time scales was underestimated by the model.

Sulfate aerosol formation is thought to be initiated mainly by binary homogeneous nucleation of $H_2SO_4$ and $H_2O$ vapors, primarily in the tropical tropopause region. The aerosol size distribution is modified by condensation and evaporation of gas-phase $H_2SO_4$ and by coagulation among particles (Brock et al. 1995; Hamill et al., 1997). Sulfate aerosol particles are assumed to be liquid spheres with equilibrium composition ($H_2SO_4$ and $H_2O$ fractions) determined by the local grid box temperature and water vapor concentration (Tabazadeh et al., 1997). The model uses a sectional representation of particle sizes, with 40 logarithmically-spaced sulfate aerosol bins, representing sizes from 0.39 nm to 3.2 μm, with aerosol volume doubled between adjacent bins. Particle distributions are also modified by sedimentation and by rainout/washout processes in the troposphere. The sedimentation formulation is described below. Rainout/washout process are represent by a first order loss term in the troposphere with removal lifetime ranging from 5 days at the surface to 30 days at the tropopause.

Solid particles are modeled with a similar sectional representation; in this case it is the number of monomers per particle that is doubled in successive bins. Only the monomers, the primary particles directly injected into the atmosphere, are assumed spherical. Larger particles produced

Debra Weisenstein 7/13/2015 3:01 PM
**Deleted:** l

Debra Weisenstein 7/13/2015 3:04 PM
**Deleted:** , for both

Debra Weisenstein 7/13/2015 3:02 PM
**Deleted:** , and was found to be among the best 2-D and 3-D models available at that time.

Debra Weisenstein 7/13/2015 4:46 PM
**Deleted:** s

Debra Weisenstein 7/13/2015 4:45 PM
**Deleted:** are

Debra Weisenstein 7/13/2015 4:46 PM
**Deleted:** produced

Debra Weisenstein 7/13/2015 4:46 PM
**Deleted:** ,

Debra Weisenstein 7/13/2015 4:47 PM
**Deleted:** and t

Debra Weisenstein 7/13/2015 4:47 PM
**Deleted:** ir

Debra Weisenstein 7/13/2015 4:51 PM
**Deleted:** by

Debra Weisenstein 7/13/2015 4:51 PM
**Deleted:** ing

Debra Weisenstein 7/13/2015 4:53 PM
**Deleted:**

Debra Weisenstein 6/19/2015 8:51 AM
**Deleted:** emit

by coagulation assume fractal structures that obey a statistical scaling law where the fractal dimension $D_f$ determines how the size of an aggregate of particles is related to the number of primary particles (Filippov et al., 2000; Maricq, 2007). . The radius of gyration $R_g$ of a fractal (the root-mean-square distance from the center of mass) is given by:

$$R_g = R_0 (N_i/k_f)^{(1/D_f)}$$

where $R_0$ is the primary particle radius, $N_i$ the number of monomers in the fractal of bin i, and $k_f$ is a prefactor. Thus particle mass is proportional to $R_g^{D_f}$. The fractal dimension $D_f$ for a given material has been found to be invariant for a wide range of $R_0$ and $N_i$ values.

The surface area (S) for a fractal particle can be parameterized with an effective radius $R_{eff}$ which can be related to primary radius and the number of monomer cores in the particle:

$$R_{eff} = R_0 (N_i/k_h)^{(1/D_h)}$$

$$S_i = (4 \pi R_0^2) * (N_i/k_h)^{(2/D_h)}$$

where $D_h$ and $k_h$ are the scaling exponent and prefactor specific to surface transfer processes. With fractal dimension $D_f < 2.0$, $D_h$ can be assumed equal to 2.0. With $D_f > 2.0$, $D_h$ can be assumed equal to $D_f$ (Filippov et al., 2000). When $D_h = 2.0$, the surface area of a fractal particle is equal to the surface area of the monomer multiplied by the number of monomers in the aggregate. This formalism is most appropriate for large values of $N_i$ (i.e., greater than 100). For consistency at small values of $N_i$, we assume that $k_f = k_h = 1$, since we find that simulations producing only small $N_i$ values are most efficient for geoengineering.

The solid particles are allowed to interact with background stratospheric sulfate particles by coagulation, and with gas phase $H_2SO_4$ and $H_2O$ by condensation and evaporation. We use $R_g$ as the particle radius when calculating the coagulation kernel, the probability that two particles will combine into one on collision (Maricq, 2007). The coagulation formulation between and among different particle types is detailed in Appendix A. The condensation rate, also detailed in Appendix A, depends on particle surface area, and secondarily, on a radius of curvature for the Kelvin correction. We use $R_0$ as the radius-of-curvature in the condensation equation, since gas molecules see the individual monomers making up the fractal. We model mixed-phase particles by tracking particle number per bin and mass of $H_2SO_4$ per bin in the mixed particles. Volume and surface area of the mixed particles depends also on the $H_2O$ present in the equilibrium

Debra Weisenstein 7/9/2015 4:00 PM
**Deleted:** that are defined by a

Debra Weisenstein 7/9/2015 4:01 PM
**Deleted:** that

Debra Weisenstein 7/13/2015 4:58 PM
**Moved (insertion) [3]**

Debra Weisenstein 7/13/2015 4:58 PM
**Moved up [3]:** (Filippov et al., 2000; Maricq, 2007).

Debra Weisenstein 7/9/2015 4:05 PM
**Moved (insertion) [2]**

Debra Weisenstein 6/28/2015 11:03 PM
**Deleted:** S

Debra Weisenstein 6/28/2015 11:03 PM
**Deleted:** density

Debra Weisenstein 6/28/2015 11:02 PM
**Deleted:** AD

Debra Weisenstein 7/20/2015 2:39 PM
**Deleted:** s

Debra Weisenstein 6/28/2015 11:02 PM
**Deleted:** AD

Debra Weisenstein 7/20/2015 2:47 PM
**Moved down [4]:** Above about 35 km, coated particles will lose their sulfate coating by evaporation and become dry again.

$H_2SO_4$-$H_2O$ solution. Above about 35 km, coated particles will lose their sulfate coating by evaporation and become dry again.

The sedimentation velocity of fractal particles represents a balance between the gravitational force, proportional to particle mass, $M_p$, and the drag force, proportional to the particle velocity and the two-dimensional surface area projection of the particle, $A_{2D}$, and inversely proportional to the particle radius $R_p$. Sedimentation velocity is modified by the Cunningham slip-flow correction, G, which accounts for larger sedimentation velocities with lower air density (Seinfeld and Pandis, 2006). We obtain sedimentation velocity $W_{sed}$ from

$$W_{sed} = (M_p\, g\, R_p\, G) / (6\, \eta\, A_{2D}),$$

where $\eta$ is the viscosity of air and g the gravitational constant. For spheres, $W_{sed}$ is proportional to $R_p^2$. For all fractal cases, $R_p$ is taken to be $R_g$, and with $D_f \geq 2$, the area projection is taken to be $\pi R_g^2$ yielding a $W_{sed}$ proportional to $G*N_i^{(D_f-1)/D_f}$. With $D_f < 2$, the fractal is porous and the area projection is $N_i*\pi R_0^2$, yielding a $W_{sed}$ proportional to $G*N_i^{(1/D_f)}$ (Johnson et al., 1996). For coated particles, the particle mass, $M_p$, is the sum of the solid particle mass and $H_2SO_4$-$H_2O$ mass, and particle radius is taken to be $R_g$ increased by the thickness of a uniform coating. However, when the radius of a sphere enclosing the total particle volume is larger than $R_g$ plus a monolayer of $H_2SO_4$, we use the spherical radius rather than $R_g$.

## 3 Model Results

Before turning to the results, we use the following sub-section to describe (and provide some rationale for) the solid aerosol particles that we choose as test cases, and then in Section 3.2 we describe a few results regarding the sedimentation of aggregates that are useful in understanding the model results.

### 3.1 Test cases: Alumina and diamond aerosol particles

Several prior studies have examined a range of possible solid aerosols and performed some simple optimizations (Teller et al., 1997; Pope et al., 2012; Blackstock et al., 2009). For simplicity we only considered spherical dielectric particles made of materials that have

Debra Weisenstein 7/20/2015 2:47 PM
**Moved (insertion) [4]**

Debra Weisenstein 7/20/2015 2:48 PM
**Deleted:** Volume and surface area of the mixed particles depends also on the $H_2O$ present in the equilibrium $H_2SO_4$-$H_2O$ solution.

Debra Weisenstein 5/27/2015 2:49 PM
**Deleted:** $R_g$

Debra Weisenstein 5/28/2015 10:31 AM
**Deleted:** ,

Debra Weisenstein 5/28/2015 10:32 AM
**Deleted:** whereas for uncoated fractal particles

Debra Weisenstein 5/28/2015 10:33 AM
**Deleted:** and

Debra Weisenstein 5/28/2015 10:33 AM
**Deleted:** is

Debra Weisenstein 5/28/2015 10:34 AM
**Deleted:** hen

Debra Weisenstein 5/28/2015 10:34 AM
**Deleted:** We take the Reynolds number (a factor in the drag coefficient) and the Knudsen number (the primary term in the Cunningham slip-flow correction) to be proportional to $R_g$ in all fractal cases.

negligible solubility in the aqueous sulfuric acid found under typical stratospheric conditions. An ideal material for SRM would have (a) a high index of refraction, (b) a relatively low density, (c) negligible absorption for both solar and thermal infrared spectral regions, and finally (d) it should have well understood surface chemistry under stratospheric conditions. In addition, even though this research is exploratory, materials are more plausible as candidates for deployment for SRM if they have low and well understood environmental toxicity and if there is a track record of production of industrial quantities of the material in the appropriate half micron size regime.

We chose alumina, or aluminum oxide ($Al_2O_3$), as our primary test case because it has a relatively high index of refraction (n=1.77 in the middle of the solar band) and because there is a substantial literature on its chemistry (Molina et al., 1997; Sander et al., 2011) and stratospheric chemical impact (Danilin et al., 2001; Jackman et al., 1998). However, alumina has infrared absorption bands in the thermal infrared that will reduce its net radiative forcing and will cause some heating of the lower stratosphere (Ross and Schaeffer, 2014).

We chose diamond as a secondary test case because of its near-ideal optical properties: it has a very high index (n=2.4) and negligible absorption for both solar and thermal infrared spectral regions. Despite this we did not choose diamond as the primary test case because there is minimal data about the chemistry of relevant compounds on diamond surfaces under stratospheric conditions, and also, while industrial synthetic submicron diamond is now available at under 100 USD per kilogram, there is still far less industrial heritage on diamond production to assess the challenges of scaling production technologies to hundreds of thousands of tons per year.

Alumina is an important industrial material as a precursor for aluminum production and for a variety of uses from sunscreen compounds applied to the skin to industrial catalysis. The global production rate is approximately 100 Tg $yr^{-1}$ (USGS, 2014). There is a very large body of experience in making alumina nanoparticles. For example, liquid-feed flame spray pyrolysis is used to make structured nanoparticles of alumina in quantities greater than 1 kt $yr^{-1}$ (Hinklin et al., 2004). As we will see, the optimal size for a spherical alumina particles used as a scatterer in the stratosphere is of order 200 nm radius. Most of the industrial effort is focused on making smaller particles for catalysis but there are examples of production of relatively monodisperse particles with radii greater than 50 nm (Hinklin et al., 2004; Tsuzuki and McCormick, 2004).

Debra Weisenstein 7/21/2015 5:15 PM
**Deleted:** ,

Debra Weisenstein 7/21/2015 3:02 PM
**Deleted:** because the ability to produce sub-micron material at industrial scale is much less certain than it is for alumina

Debra Weisenstein 7/21/2015 12:48 PM
**Deleted:** Mt yr

Debra Weisenstein 8/13/2015 4:33 PM
**Deleted:**

For the purposes of this paper we will assume that it is possible to make roughly spherical alumina particles with a size range between 50 and 400 nm radius. This is a working assumption that seems plausible based on the very large technical literature (> 1,000 papers in the last decade on alumina nanoparticles) and industrial base devoted to production of these materials. But it is simply an assumption. A significant effort involving experts from industry and academia would be required to meaningfully assess the difficulty of producing large quantities of alumina with a suitable size and morphology for solar geoengineering.

There is rapidly growing industrial production of sub-micron diamond powders (Krueger, 2008), so there is no doubt that particles with appropriate morphology can be produced. However, the industrial production volumes and academic literature on production technologies are far smaller than for alumina.

Table 1 lists the numerical experiments performed for this study with the AER 2-D model. Simulations with alumina particles employ a range of injected monomer sizes, from 80 to 320 nm in radius. These simulations allow us to analyze the trade-offs between sedimentation rate, radiative forcing, and ozone depletion. For diamond, we perform simulations only for injected monomer sizes of 160 nm, near the radiative optimum. We also repeat simulations performed by Pierce et al. (2010) for geoengineering injections of $SO_2$ and $H_2SO_4$. A range of injection rates is used for each injected substance and each injected monomer radius to test linearity of the response. Each scenario is calculated with a 10 year integration period, using dynamical fields representing the 1978-2004 average repeated each year and fixed boundary conditions from approximately the year 2000, until an annually-repeating result is achieved. We analyze results from the final year of each calculation, concentrating on annual average conditions.

### 3.2 Factors controlling settling of aggregates

As discussed above, the dynamics of aggregated particles depend on their fractal dimension $D_f$. No observational data on the fractal dimension of ~100 nm hard spheres aggregating under stratospheric conditions is available. As a guide, we adopt the value of $D_f$ obtained in studies of the formation of fractal alumina aggregates from much smaller monomers at atmospheric pressure produced by combustion and oxidation of liquid aluminum drops that can result from burning solid rocket fuel. These studies, which produced aggregates of approximately 1 μm

composed of primary particles of a few tens of nanometers in diameter, determined that the fractal dimension $D_f$ for alumina is 1.60±0.04 (Karasev et al., 2001; 2004), implying a sparsely-packed fractal. For comparison, soot aggregates typically have $D_f$ values of ~2.0 (Kajino and Kondo, 2011; Maricq and Nu, 2004), while a value of 3.0 is appropriate for liquid particles which remain spherical upon coagulation. The density of alumina particles is taken to be 3.8 g $cm^{-3}$ and that of diamond to be 3.5 g $cm^{-3}$. We assume the same fractal dimensions for diamond as for alumina.

Sedimentation velocity strongly influences stratospheric lifetimes. Figure 1(a) shows annual average sedimentation velocities in the tropics as a function of altitude for uncoated alumina particles for monomer radii from 80 to 320 nm. Shown are sedimentation velocities for individual monomers and for fractals with N=4 and N=32, all with fractal dimension $D_f$=1.6. N=32 fractals are not shown for monomers larger than 160 nm because significant numbers of such fractals do not form in our simulations, however we do show N=256 fractals with 80 nm monomers. Alumina monomers fall at a faster rate than sulfate particles of the same diameter, given their greater density (3.8 g $cm^{-3}$ for $Al_2O_3$, approximately 1.7 g $cm^{-3}$ for stratospheric $H_2SO_4$-$H_2O$ particles), and diamond particles (not shown) fall only slightly slower than alumina particles of the same radius owing to 8% smaller density. Fractal particles fall faster than the monomers they are composed of in the troposphere and lower stratosphere, but at the same rate in the middle and upper stratosphere where the Knudsen number Kn > 1 and the slip-flow correction has the opposite size dependence as the other terms. Figure 1 also shows the model's average upward advective velocity in the tropics as a function of altitude for comparison. Where sedimentation velocity exceeds average upwelling velocity, we expect alumina lifetime and vertical extent to be greatly impacted. This occurs only above 30 km for 80 nm monomers, but above 24 km for 160 nm monomers and 19 km for 240 nm monomers. For 240 nm and 320 nm monomers injected into the tropics at 20-25 km altitude, only a fraction of the injected mass will be lofted to higher altitudes and distributed to high latitudes by the Brewer-Dobson circulation.

It is known that soot particles, which form fractals similar to alumina particles, eventually assume a more compact structure in the atmosphere after acquiring a liquid coating (Kajino and Kondo, 2011; Mikhailov et al., 2006). Observations on the liquid uptake properties of alumina and their potential shape compaction are not available. For simplicity, we assume that the alumina particles are hydrophobic until they are coated with a sulfate-water mixture by

Debra Weisenstein 7/9/2015 4:05 PM
**Moved up [2]:** The fractal dimension for a given material has been found to be invariant for a wide range of $R_0$ and $N_i$ values.

Debra Weisenstein 5/27/2015 8:56 AM
**Deleted:** /

Debra Weisenstein 5/27/2015 8:56 AM
**Deleted:** /

Debra Weisenstein 7/10/2015 3:54 PM
**Deleted:** no

Debra Weisenstein 7/10/2015 3:55 PM
**Deleted:** large

Debra Weisenstein 5/28/2015 1:47 PM
**Deleted:** size

coagulation with existing sulfate particles, and then they may take up additional $H_2SO_4$ and $H_2O$ by condensation. The effects of this assumption are expected be small under non-volcanic conditions, as most (>95%) stratospheric sulfate mass exists in condensed form. To test the potential effect of compaction of liquid-coated solid alumina particles, we perform additional model calculations assuming that the wetted particles change their fractal dimension $D_f$ from 1.6 to 2.8, and their surface area scaling exponent $D_h$ from 2.0 to 2.8, likely the maximum compaction that could be achieved. While a time lag from initial wetting to shape compaction may be appropriate, we assume instantaneous compaction on wetting for calculations labeled "compact coated" as a way to bracket the effect. When the compacted particles lose their $H_2SO_4$ by evaporation, they are assumed to retain their compact shape. Sedimentation velocities for these coated and compacted particles are shown in Fig. 1(b). In this case, higher order fractals fall at faster velocities than their respective monomers at all altitudes, which will affect the residence time of alumina and its calculated atmospheric burden.

Debra Weisenstein 6/28/2015 11:03 PM
**Deleted:** SAD

Debra Weisenstein 8/14/2015 11:46 AM
**Deleted:** life

### 3.3 Aerosol distribution and burden

We model geoengineering by injection of alumina particles for a number of parametric model scenarios to evaluate the effect of (1) injected particles size, (2) injection rate, and (3) the fractal geometry of sulfate-coated alumina particles. For all scenarios, injection occurs in a broad band from 30°S to 30°N and from 20-25 km in altitude. This is the same injection region used in Pierce et al. (2010) and was chosen to maximize the global distribution and residence time of geoengineered aerosols while minimizing localized injection overlaps. We assume that it is feasible to emit alumina particle monomers with a uniform diameter, either by a flame process at the injection nozzle or by releasing prefabricated particles. Particles are released continuously at injection rates of 1, 2, 4, or 8 Tg per year, all as monomers of a single radius (80 nm, 160 nm, 240 nm, or 320 nm), as detailed in Table 1. Stratospheric particle injections are continuous in time and the simulations are continued for 10 years until a steady atmospheric concentration is reached. Alumina particles that become coated with sulfate are treated either as retaining their sparse structure with fractal dimension $D_f$ of 1.6 or instantaneously becoming more compact fractal particles with $D_f$ of 2.8. We use a 2-D model for computation efficiency in this first evaluation of geoengineering by solid particle injection, and thus we implicitly mix the injected

Debra Weisenstein 7/21/2015 12:49 PM
**Deleted:** Mt

Debra Weisenstein 6/18/2015 1:29 PM
**Deleted:** Emissions

Debra Weisenstein 8/14/2015 11:53 AM
**Deleted:** approximately

material into zonally-uniform bands dictated by the model's spatial resolution of 9.5 degrees latitude by 1.2 km altitude. The impact of this simplification, along with the neglect of enhanced coagulation in injection plumes, will be discussed in Section 4.

We first examine the calculated concentration and size distribution of atmospheric alumina under a geoengineering scenario with an injection rate of 1 Tg $yr^{-1}$, assuming no particle compaction on coating with sulfate. Figure 2, top panels, shows the mass mixing ratio of alumina (ppbm) with injections of 80 nm monomers and 240 nm monomers. Significant alumina concentration exist up to 40 km altitude when 80 nm particles are injected, but only below 30 km for injection of 240 nm particles due to the difference in sedimentation speeds. The peak mass mixing ratio of alumina with 80 nm monomers injected is 40% larger than that with 240 nm monomers injected. The lower panels of Fig. 2 show the concentration of particles ($cm^{-3}$) for the same cases. Particle concentrations of up to 25 $cm^{-3}$ are found for 1 Tg $yr^{-1}$ injection of 80 nm monomers but remain less than 3 $cm^{-3}$ for injection of 240 nm monomers. The particle concentration drops away from the injection region as the monomers coagulate into fractals and have time to settle downward. The low number densities with $R_0$=240 nm result in minimal coagulation between alumina particles.

The distribution of stratospheric alumina mass into monomers and fractals is shown in Fig. 3 at the equator with 80 nm monomers injected (panel a) and for the global average with 80, 160, and 240 nm monomers injected (panels b-d), all with 1 Tg $yr^{-1}$ of emissions. With injection of 80 nm monomers, 27% of the mass remains in monomers at the equator, with no more than 13% of the mass in any size bin with 2 or more monomers in the fractal. Some fractal particles comprised of 1024 monomers exist. At higher latitudes, the monomer fraction drops and the proportion in higher order fractals increases, as seen in the global average (panel b). The fraction of monomers coated, shown as the blue portion of each bar, increases with distance from the tropical injection region. Coated fractions also increase with increasing numbers of monomers per fractal particle. This reflects both the longer residence time of the larger particles and their large cross-section, which enhances coagulation with sulfate particles. Virtually all of the alumina mass is coated for fractals with more than 128 monomers per particle. Alumina in the troposphere is almost all coated with sulfate due to the large sulfate concentrations there, though alumina concentrations are small. With injection of 160 nm alumina monomers, 71% of the global mass remains in monomers, and fractals composed of only 2-16 monomers are found in

Debra Weisenstein 7/21/2015 12:48 PM
**Deleted:** Mt yr

Debra Weisenstein 7/10/2015 1:53 PM
**Deleted:** atmospheric concentration

Debra Weisenstein 8/14/2015 11:57 AM
**Deleted:** Total stratospheric burden

Debra Weisenstein 8/14/2015 11:59 AM
**Deleted:** almost double

Debra Weisenstein 7/21/2015 12:48 PM
**Deleted:** Mt yr

Debra Weisenstein 7/21/2015 12:48 PM
**Deleted:** Mt yr

significant concentrations. Results for diamond closely resemble those for alumina with 160 nm monomers injected. With injection of 240 nm alumina monomers, 94% of the mass remains in monomers, and with 320 nm monomers injected, 98% is monomers. Larger fractions of the alumina mass are coated in these latter cases.

The mass fraction in monomers versus higher order fractals varies with injection rate. Figure 4(a) shows mass fraction vs the number of monomers per particle for injection of 80 nm monomers at rates varying from 1 Tg $yr^{-1}$ to 8 Tg $yr^{-1}$. The 1 Tg $yr^{-1}$ cases (green lines) match the global mass fractions shown in Figure 3. As the injection rate increases, the mass fraction of monomers decreases while the peak distribution shifts to larger fractals. At injection rates of 2, 4, and 8 Tg $yr^{-1}$, the size distribution peaks at 32, 64, and then 128 monomers per particle, and fractals composed of 2000 monomers are found. Figure 4(b) shows a similar figure with injection of alumina as 160 nm radius monomers. Because these particles contain 8 times the mass of the 80 nm monomers, particle concentrations are considerably smaller and coagulation less effective. Fractals containing more than 128 monomers do not occur in significant concentrations, even with 8 Tg $yr^{-1}$ of emission. For injection of 240 nm monomers (Fig. 4c), 70% of the particles remain as monomers even with 8 Tg $yr^{-1}$ of emission, and fractals exceeding 16 monomers exist at only insignificant concentrations. For injection of 320 nm monomers (not shown), significant concentrations are found only for monomers and fractals composed of 2 and 4 monomers even with 8 Tg $yr^{-1}$ of emission.

Figure 5(a) shows the stratospheric alumina burden as a function of injection rate for four different radii of injected monomers. Alumina burden is seen to be approximately linear with injection rate. This is in contrast to a more strongly decreasing rate of change with increasing injection rate seen for geoengineering by injection of $SO_2$ or $H_2SO_4$, also shown in Fig. 5(a). In the case of sulfur injection, particles that grow to larger spherical sizes have shorter atmospheric residence times. For alumina particles with sparse fractal structure ($D_f$=1.6), the fractal particles do not increase their sedimentation velocities in the middle and upper stratosphere as they grow by coagulation, resulting in residence times remaining almost constant over the alumina size distribution. The cases that produce the fewest fractals ($R_0$=240 and 320 nm) have the most linear response. The calculated atmospheric burden for diamond (not shown) is almost identical to that for alumina of the same size injected monomer. Also shown in Fig. 5 as dashed lines are simulations with coated alumina particles assumed to adopt a more compact fractal shape



Debra Weisenstein 7/21/2015 12:48 PM
**Deleted:** Mt yr

Debra Weisenstein 7/21/2015 12:48 PM
**Deleted:** Mt yr

Debra Weisenstein 7/21/2015 12:48 PM
**Deleted:** Mt yr

Debra Weisenstein 7/2/2015 8:28 AM
**Deleted:** never

Debra Weisenstein 7/21/2015 12:48 PM
**Deleted:** Mt yr

Debra Weisenstein 7/21/2015 12:48 PM
**Deleted:** Mt yr

Debra Weisenstein 7/2/2015 8:40 AM
**Deleted:** no

Debra Weisenstein 7/2/2015 8:36 AM
**Deleted:** no

Debra Weisenstein 7/2/2015 8:38 AM
**Deleted:** exceed

Debra Weisenstein 7/2/2015 8:34 AM
**Deleted:** particle

Debra Weisenstein 7/21/2015 12:48 PM
**Deleted:** Mt yr

Debra Weisenstein 8/14/2015 12:10 PM
**Deleted:** monomer

Debra Weisenstein 8/17/2015 4:28 PM
**Deleted:** emission

Debra Weisenstein 8/17/2015 4:28 PM
**Deleted:** emissions

Debra Weisenstein 8/14/2015 2:07 PM
**Deleted:** (Heckendorn et al., 2009)

Debra Weisenstein 8/14/2015 2:07 PM
**Deleted:** (Pierce et al., 2010)

Debra Weisenstein 8/14/2015 12:12 PM
**Deleted:** larger

($D_f$=2.8). For these scenarios, total stratospheric burden is reduced due to the faster sedimentation of the coated fractal particles, while the mass fraction in monomers is increased due to fewer high-order fractals to scavenge the monomers. Only the 80 nm and 160 nm cases show significant differences under the assumption that coated particles become more compact.

The stratospheric burden of sulfate is shown in Fig. 5(b) under various geoengineering scenarios with alumina injection. Thick lines (left hand axis labels) represent the total stratospheric burden of condensed sulfate as a function of geoengineering injection rate of alumina while thin lines (right hand axis labels) represent the fraction of stratospheric liquid sulfate on the surface of alumina particles. With injection of 80 nm alumina monomers, total stratospheric sulfate increases above background for injections less than 1.5 Tg $yr^{-1}$, but then decreases with higher injection rates. Up to 86% of the total stratospheric sulfate is found on alumina particles in these cases, a result of the large alumina surface area available and high coagulation rates with large fractals. Alumina injection cases with larger monomer diameters lead to decreases in the total stratospheric burden of liquid sulfate because of the faster sedimentation of the larger alumina particles along with their sulfate coatings. The maximum decrease in total stratospheric sulfate is about 30%. The fraction of total stratospheric sulfate found on alumina particles is as much as 82% with 160 nm monomers, 61% with 240 nm monomers, and 32% with 320 nm monomers. The calculated thickness of the sulfate coating on alumina particles in the stratosphere varies from 5 to 15 nm with 80 nm monomers and from 10 to 40 nm with 240 nm monomers with 1 Tg $yr^{-1}$ of injection. However, as the geoengineering injection rate increases, the sulfate layer on alumina particles becomes thinner since the stratospheric sulfate burden will then be distributed over a larger alumina surface area.

Debra Weisenstein 7/21/2015 12:48 PM
**Deleted:** Mt yr

Debra Weisenstein 7/21/2015 12:48 PM
**Deleted:** Mt yr

Debra Weisenstein 8/17/2015 4:29 PM
**Deleted:** emission

### 3.4 Radiative forcing assessment

Alumina particles are known to be more efficient scatterers than sulfate particles, and thus are expected to be more efficient per unit mass for geoengineering applications. Figure 6 compares the Mie scattering properties in the solar band of alumina and diamond monomers and sulfate particles as a function of particle radius. We calculated the solid particle monodisperse single scatter albedo values from Mie Theory (Bohren and Huffman 2008) using tabulated complex refractive index data for diamond (Edwards and Philipp 1985) and alumina (Thomas and Tropf

1997). The upscatter and downscatter cross sections are calculated from Wiscombe and Grams (1976), utilizing the scattering phase function from Mie Theory and the same complex refractive index data. Figure 6(a) shows the ratio of upscatter cross section to geometric cross-section for the three particle types. The sulfate profile is fairly flat, with a cross section of about 0.3 for particles greater than 0.5 μm, whereas the alumina profile shows a 30% drop from its peak of 0.6 between 0.2 μm and 0.6 μm to 0.4 at 2 μm. The diamond profile shows a peak of 0.9 between 0.15 and 0.5 μm, dropping to about 0.55 at radii greater than 1.2 μm. Figure 6(b) shows strong peaks in upscatter per unit volume for alumina and diamond monomers as a function of radius. In contrast, sulfate particles exhibit a much flatter function of upscatter per unit volume as a function of radius. Alumina monomers scatter most efficiently per unit particle volume at about 200-250 nm. At this radius, they have three times the upscatter per unit volume as sulfate particles. Upscatter per unit mass however, due to the difference in density of alumina relative to sulfate, shows less contrast. For diamond monomers, the upscatter per unit volume peaks at around 150 nm radius, with over twice the peak upscatter of alumina monomers. Figure 6(c) shows the ratio of downscatter cross section to upscatter cross section for alumina, diamond, and sulfate as a function of radius. Alumina monomers have about half the downscatter per unit of upscatter as sulfate particles, while diamond monomers have half the downscatter of alumina. Thus in geoengineering applications, alumina and diamond would scatter radiation back to space and produce substantially smaller increases in diffuse radiation at the surface than would sulfate particles producing the same change in RF.

We use a scattering code which integrates the Mie scattering function over shortwave spectral bands and scattering angles as a function of particle size (monomers and fractals) using an efficient impulse-function method. Multiple scattering is ignored as solid particle optical depths are small. For purposes of radiative forcing, we assume that solid particles with thin sulfate coatings behave the same as bare particles. We follow Rannou et al. (1999) for scattering by fractals, and follow the approximation in Charlson et al. (1991) by scaling our calculated RF values by $(1-\alpha)^2$, where $\alpha$ represents surface albedo, here taken to be 0.2. Figure 7(a) shows the shortwave globally-averaged clear-sky radiative forcing functions, in W $m^{-2}$ per Tg of aerosol burden, obtained by our scattering code as a function of monomer radius and fractal size (number of cores per particle). Scattering by 80 nm alumina monomers is much less efficient (factor of 4) than scattering by 160 nm alumina monomers. There is little difference in scattering between

Debra Weisenstein 7/29/2015 3:50 PM
**Deleted:** s

Debra Weisenstein 8/24/2015 5:44 PM
**Deleted:**

Debra Weisenstein 7/21/2015 5:19 PM
**Deleted:** without a simultaneous significant

Debra Weisenstein 7/29/2015 3:52 PM
**Deleted:** Mie

Debra Weisenstein 5/28/2015 2:14 PM
**Deleted:**

Debra Weisenstein 7/29/2015 3:55 PM
**Deleted:** (

Debra Weisenstein 7/21/2015 12:49 PM
**Deleted:** Mt

Debra Weisenstein 7/29/2015 3:55 PM
**Deleted:** $^{-1}$)

240 nm and 320 nm alumina monomers, both with about 50% greater RF per terragram burden than 160 nm monomers. Fractals scatter much less efficiently than monomers. A fractal aggregate of two cores scatters only 50% as much radiation per unit mass as a corresponding monomer, and higher order fractals scatter even less efficiently. An aggregate of 16 alumina monomers has negligible scattering per unit mass. The functions with fractal dimension of both $D_f$ =1.6 (solid lines) and $D_f$ =2.8 (dashed lines, labeled "compact coated") are shown for alumina, however, this produces only a minor difference in radiative forcing per unit mass. The radiative forcing function for diamond with 160 nm monomers (the radius of peak backscatter efficiency) shows significantly greater forcing than alumina, 2.7 times greater than 160 nm alumina monomers and 1.8 times greater than 240 nm alumina monomers.

We obtain averages of solid aerosol mass in each bin size (monomers and fractals) integrated vertically and averaged over latitude and season. The integrated and averaged aerosol mass per bin is multiplied by the spectrally-integrated radiative forcing per terragram burden for each bin to obtain the total radiative forcing for each geoengineering scenario. The global annual average top-of-atmosphere shortwave radiative forcing due to alumina and diamond is shown in Fig. 7(b) as a function of injection rate for specified sizes of injected monomers under clear sky conditions. We choose to present only shortwave radiative forcing as more relevant to geoengineering intended to offset surface warming after atmospheric adjustments. However, the longwave radiative forcing is only about 10% of the shortwave RF for alumina, though of opposite sign, and is negligible for diamond.

For alumina, shortwave RF for cases with 80, 160, 240, and 320 nm injected monomer size are shown in Fig. 7(b) as a function of injection rate. Cases with 80 nm monomer injections have very low RF, due both to inefficient scattering for monomers of that size, and the large proportion of fractals to monomers. The RF for the 80 nm injection case increases very little with increasing injection rate, as increasing injections produce fractals composed of more than 64 monomers which produce almost no scattering per unit mass. The case with injection of 320 nm alumina monomers produces less RF than the case with injection of 240 nm alumina monomers. Though monomers of 320 nm produce slightly more RF per terragram than monomers of 240 nm, the 320 nm injection cases yield a smaller burden due to their faster sedimentation rates. Injection of 240 nm monomers is found to produce the most radiative forcing per terragram of alumina injected annually, consistent with the peak of the upscatter per

Debra Weisenstein 7/24/2015 4:33 PM
**Deleted:** megaton

Debra Weisenstein 7/24/2015 10:28 PM
**Deleted:** megaton

Debra Weisenstein 7/21/2015 2:58 PM
**Deleted:** megaton

Debra Weisenstein 5/28/2015 2:15 PM
**Deleted:** For purposes of radiative forcing, we assume that solid particles with thin sulfate coatings behave the same as bare particles.

Debra Weisenstein 7/24/2015 10:28 PM
**Deleted:** megaton

Debra Weisenstein 7/26/2015 11:45 PM
**Deleted:** the

Debra Weisenstein 7/26/2015 11:47 PM
**Deleted:**

Debra Weisenstein 7/26/2015 11:45 PM
**Deleted:** injections

Debra Weisenstein 7/26/2015 11:48 PM
**Deleted:**

Debra Weisenstein 8/17/2015 4:29 PM
**Deleted:** emissions

Debra Weisenstein 8/17/2015 4:29 PM
**Deleted:** emission

Debra Weisenstein 8/11/2015 7:06 PM
**Deleted:** s

Debra Weisenstein 7/24/2015 10:29 PM
**Deleted:** megaton

Debra Weisenstein 7/24/2015 10:29 PM
**Deleted:** megaton

Debra Weisenstein 7/24/2015 10:30 PM
**Deleted:** megaton

Debra Weisenstein 8/17/2015 4:30 PM
**Deleted:** emissions

unit volume curve shown in Fig. 6(b). We calculate radiative forcing for diamond injections of 160 nm monomers only, also shown in Fig. 7(b). Atmospheric burden of diamond is very similar to that for alumina of the same radius, but RF is much larger owing to more efficient scattering. Diamond injection at a rate of 4 Tg $yr^{-1}$ results in -1.8 W $m^{-2}$ of shortwave forcing, while the same alumina injection results in only -1.2 W $m^{-2}$ of shortwave forcing. The increase in downward diffusive flux is also calculated by our radiative forcing code and is shown in Table 2 for selected cases which each produce -2 W $m^{-2}$ of shortwave radiative forcing. For equivalent radii and injection rate, diamond produces up to twice the diffuse downward radiation as alumina, however, per unit change in top-of-atmosphere shortwave radiative forcing, diamond produces less diffuse downward radiation.

Our method produces only a globally-averaged value of radiative forcing by solid particles. Our results are not meant to be of high accuracy, as they do not account for clouds or molecular scattering and are limited by the index of refraction data, uncertainties in fractal scattering, and our averaging method. Nevertheless, it is useful to obtain well-founded estimates of radiative forcing for comparison with sulfate geoengineering, and relative efficiencies among solid particle scenarios as a function of injected monomer diameter. The RF plot in Fig. 7(b) shows clear sky shortwave radiative forcing from two sulfur geoengineering scenarios as well. The scenario results were calculated with the AER 2-D model, as applied in Pierce et al. (2010) but using the radiative scattering code applied to alumina and diamond. Note that we plot them here relative to the total $SO_2$ or $H_2SO_4$ injection mass per year, not the sulfur mass injected per year. The most efficient alumina geoengineering scenario, with 240 nm monomers injected, has roughly the same RF efficiency per terragram of injection as geoengineering by injection of $H_2SO_4$. However, if a geoengineering methodology were to transport only sulfur to the stratosphere and create $H_2SO_4$ in situ, then sulfur geoengineering would be more efficient than alumina per terragram per year transported.

Aerosol heating of the tropical lower stratosphere is another potential risk of geoengineering. Heckendorn et al. (2009) investigated this effect and the resulting increase in stratospheric water vapor, primarily caused by longwave heating, for sulfate aerosol. To estimate lower stratospheric heating by solid particles, we use the Rapid Radiative Transfer Model (RRTM) developed by Atmospheric and Environmental Research (Mlawer et al. 1997; Clough et al. 2005) to calculate radiative heating rates for mean cloud-free tropical atmospheric profiles with and

Debra Weisenstein 7/31/2015 10:31 AM
**Deleted:** a

Debra Weisenstein 7/21/2015 12:48 PM
**Deleted:** Mt yr

Debra Weisenstein 7/29/2015 8:00 PM
**Deleted:** 2.0

Debra Weisenstein 7/29/2015 8:00 PM
**Deleted:** 3

Debra Weisenstein 5/26/2015 5:44 PM
**Deleted:** 1

Debra Weisenstein 7/31/2015 12:12 PM
**Deleted:**

Debra Weisenstein 8/24/2015 5:32 PM
**Deleted:** ballpark

Debra Weisenstein 6/19/2015 8:48 AM
**Deleted:** emitt

Debra Weisenstein 7/31/2015 12:47 PM
**Deleted:** Heckendorn et al. (2009) and

Debra Weisenstein 6/19/2015 8:49 AM
**Deleted:** emit

Debra Weisenstein 7/24/2015 10:30 PM
**Deleted:** megaton

Debra Weisenstein 8/21/2015 12:52 PM
**Deleted:** emissions

Debra Weisenstein 7/24/2015 10:31 PM
**Deleted:** megaton

Debra Weisenstein 7/31/2015 12:58 PM
**Deleted:** Longwave, or infrared (IR),

Debra Weisenstein 7/31/2015 12:58 PM
**Deleted:** in

Debra Weisenstein 8/20/2015 1:09 PM
**Deleted:** stratosphere, particularly in the

Debra Weisenstein 8/20/2015 1:09 PM
**Deleted:** ,

Debra Weisenstein 7/31/2015 1:00 PM
**Deleted:** this effect

Debra Weisenstein 8/25/2015 9:14 AM
**Deleted:** a

Debra Weisenstein 7/31/2015 1:30 PM
**Deleted:** infrared

Debra Weisenstein 8/19/2015 4:33 PM
**Deleted:** and top of the atmosphere shortwave radiative forcing

without a uniform aerosol density of 1 $cm^{-3}$ between 18 and 23 km. The combined longwave and shortwave heating rates shown in Table 2 for alumina, diamond, and sulfate are generated by scaling the RRTM results for number densities of 1 $cm^{-3}$ to the average number density in the 18-23 km region between 30°S and 30°N for scenarios predicted to produce -2 W $m^{-2}$ of shortwave radiative forcing. For alumina and diamond, the RRTM calculation uses only the monomer size of 240 nm or 160 nm, respectively, ignoring fractal particles and treating coated monomers the same as uncoated monomers. The range provided for heating by alumina and diamond in Table 2 uses monomer number densities for the low estimate and total particle number densities for the high estimate as multipliers for the heating rate determined from RRTM with average number density of 1 $cm^{-3}$. For sulfate particles, we employ a size distribution due to the sensitivity of heating rates to particle diameter and the range of diameters generated in geoengineering scenarios. We find that the lower stratospheric heating rate from alumina is approximately 4-5 times less than the heating rate from sulfate, comparing scenarios which each generate -2 W $m^{-2}$ of shortwave RF. Shortwave heating from alumina is about 15% of the total heating, and from sulfate about 20%. The total heating rate from diamond is almost entirely due to shortwave effects, but is still much less than that for alumina with the same top-of-atmosphere shortwave radiative forcing.

Debra Weisenstein 7/31/2015 1:31 PM
**Deleted:** longwave

Debra Weisenstein 5/26/2015 5:45 PM
**Deleted:** 1

Debra Weisenstein 7/31/2015 1:31 PM
**Deleted:**

Debra Weisenstein 8/20/2015 12:48 PM
**Formatted:** Superscript

Debra Weisenstein 7/31/2015 1:31 PM
**Deleted:** longwave

Debra Weisenstein 8/14/2015 3:40 PM
**Deleted:** longwave

Debra Weisenstein 8/11/2015 7:30 PM
**Deleted:** 4-

Debra Weisenstein 8/14/2015 3:42 PM
**Deleted:** , while longwave heating from diamond is minimal

### 3.5 Ozone impacts

Heterogeneous reactions on stratospheric particles play an important role in ozone chemistry by converting inactive forms of chlorine and bromine to forms that contribute directly to catalytic destruction of ozone. In addition, the heterogeneous conversion of $N_2O_5$ to $HNO_3$ reduces $NO_x$ concentrations. This increases ozone concentrations in the middle stratosphere where $NO_x$ reactions dominate the ozone loss cycles, but it decreases ozone concentrations in the lower stratosphere where $HO_x$, $ClO_x$, and $BrO_x$ loss cycles dominate. Transient increases in sulfate aerosols following volcanic eruptions have caused temporary depletions in ozone (Solomon, 1999). Geoengineering by stratospheric aerosol injection would be expected to lead to analogous ozone depletion, depending on the heterogeneous reactions that occur on the particle surfaces and their rates.

Ozone loss due to geoengineering injections of sulfate precursors has been explored by several authors (Heckendorn et al., 2009; Tilmes et al., 2008; 2009; 2012; Pitari et al., 2014). Here we provide a preliminary assessment of ozone loss from geoengineering injection of alumina and diamond solid particles. To enable a relative comparison of the ozone impact of sulfate geoengineering, we use the same model to compute changes in ozone abundance arising from injections of both solid particles and of sulfate aerosols. We use the AER 2-D chemistry-transport-aerosol model which includes full ozone chemistry, with 50 transported species, an additional 51 radical species, 286 two- and three-body chemical reaction, 89 photolysis reactions, and 16 rainout/washout removal processes coupled to our aerosol model (Weisenstein et al., 1998; 2004; Rinsland et al., 2003). Reaction rates are from the JPL compendium (Sander et al., 2011). The model parameterizes polar stratospheric clouds (PSCs) using thermodynamic equilibrium, employing the formulas of Hanson and Mauersberger (1998) and Marti and Mauersberger (1993) for equilibrium vapor pressures over solid $HNO_3$ and ice, respectively, assuming no supersaturation and prescribing the particle radii. ~~A comparison with observed~~ ozone trends between 1979 and 2000 is presented in Anderson et al. (2006) for the AER model and several other models. Our simulations of ozone change due to $SO_2$ injections are similar to those of Heckendorn et al. (2009) if we compare equivalent scenarios, but larger than those of Tilmes et al. (2012). This model does not include radiative or dynamical feedbacks; temperature and circulation are fixed with a climatology averaged over the years 1978 through 2004. Thus our evaluation of ozone changes due to geoengineering by injection of solid particles includes only chemical perturbations due to heterogeneous reactions on particle surfaces and not due to changes in temperature or dynamics induced by the geoengineering.

The amount of ozone loss induced by stratospheric aerosols is strongly dependent on the concentrations of halogen species, primarily Cl and Br. Future concentrations of halogens are expected to decline as a result of emissions controls, so the impact of stratospheric aerosols on ozone will—all else being equal—decline over time. To err on the side of caution by overstating the ozone impacts, we use present-day trace gas concentration throughout this study with 3.4 ppbv of total chlorine and 23 pptv of total bromine, including 6 pptv of inorganic bromine derived from the very short lived (VSL) organic compounds $CH_2Br_2$ and $CHBr_3$. Tilmes et al. (2012) showed that inclusion of VSL bromine increases ozone depletion in geoengineering

Debra Weisenstein 8/22/2015 6:18 PM
**Deleted:** and includes sedimentation of ice and solid NAT particles.

Debra Weisenstein 8/21/2015 3:46 PM
**Deleted:** C

scenarios. A more detailed evaluation of ozone impacts of solid particle geoengineering will await further studies with coupled aerosol-chemistry-climate models.

Aerosol surface area density (SAD in units of $\mu m^2/cm^3$) contributes to determining the rates of heterogeneous chemical reactions that occur on particle surfaces. Heterogeneous reactions may occur on bare alumina surfaces in the stratosphere, as well as on sulfate surfaces. The reaction $ClONO_2+HCl \rightarrow Cl_2+HNO_3$ has been measured on alumina surfaces (Molina et al., 1997; Sander et al., 2011) and would be expected to cause ozone depletion (Danilin et al., 2001; Jackman et al., 1998), though uncertainties in this reaction and the surface properties of alumina aerosol remain unexplored. Figure 8 shows bare alumina surface area density for the cases with 1 Tg $yr^{-1}$ injection of 80 nm monomers (left panel) and 240 nm monomers (right panel). Alumina SAD is largest in the tropics where particles are injected, and is lower at higher latitudes where a larger fraction of the surfaces are coated with sulfate. Alumina SAD extends to higher altitudes, up to 40 km and above, with injection of 80 nm monomers, whereas the 240 nm monomers and their fractal derivatives sediment fast enough to preclude significant SAD above 30 km. Note that sulfate aerosols generally evaporate above about 35 km altitude, and thus geoengineering with solid particles may introduce significant surface area density in regions that currently are not greatly impacted by heterogeneous chemistry.

Debra Weisenstein 7/21/2015 12:48 PM
**Deleted:** Mt yr

Figure 9 shows sulfate SAD from the calculated background atmosphere without geoengineering (panel a) and the increase in sulfate SAD in an atmosphere with 1 Tg $yr^{-1}$ of geoengineering injection of 80 nm alumina monomers (panel b) or 240 nm alumina monomers (panel c). While the addition of alumina particles has produced only a small change in the total stratospheric condensed sulfate (see Fig. 5b), it has produced significant increases in sulfate surface area density. This is a result of sulfate being distributed in thin layers on the surfaces of alumina particles. With injection of 80 nm monomers, the sulfate SAD has increased by factors of 2-4 in the lower stratosphere, with maximum SAD at high latitudes where significant concentration of complex alumina fractals exist to scavenge the smaller sulfate particles. With injection of 240 nm monomers, the maximum sulfate SAD occurs in the tropics as the faster sedimentation of alumina in this case results in a smaller concentration of mostly monomers at high latitudes. Figure 9 (panel d) shows the increase in sulfate SAD for a geoengineering scenario with 1 Tg $yr^{-1}$ of $SO_2$ injection as calculated by the AER 2-D model. The SAD increase is similar in

Debra Weisenstein 7/21/2015 12:48 PM
**Deleted:** Mt yr

Debra Weisenstein 7/21/2015 12:48 PM
**Deleted:** Mt yr

magnitude to the case with injection of 80 nm alumina monomers, but has a distribution similar to the 240 nm alumina injection case. A similar injection of sulfur as $H_2SO_4$, as in Pierce et al. (2010), produces more than double this SAD increase. For reactions whose rate is dominated by liquid sulfate surface area density, we would expect similar chemical ozone loss from similar changes in sulfate SAD whether due to geoengineering by $SO_2$, $H_2SO_4$, or alumina injection.

The SAD generated by alumina geoengineering is reduced when the monomer size of the injected particles increases. Optimizing the injected monomer size would be an important strategy to minimize stratospheric ozone depletion. Figure 10 illustrates this, showing annual averaged SAD between 15 and 25 km for bare alumina (panel a) and total sulfate (pure sulfate plus sulfate-coated alumina, panel b) as a function of injection rate with injections of 80, 160, 240, and 320 nm monomers. The SAD for bare alumina drops by factors of 1.8 to 3.1, depending on injection rate, when the monomer size is increased from 80 nm to 160 nm. The alumina SAD is roughly linear with injection rate, since the alumina surface area density doesn't decrease as particles coagulate when $D_h$=2.0. The total sulfate SAD (Fig. 10b) is even more dependent on monomer diameter than is the uncoated alumina SAD. Even though the burden of stratospheric sulfate on alumina varies slowly with injection rate, the sulfate SAD varies more rapidly with injection rate as the sulfate becomes spread more thinly over a greater numbers of alumina particles. The dashed lines in Fig. 10 represent cases where the coated particles take on a more compact fractal shape, and thus sediment faster, greatly decreasing sulfate SAD for the 80 and 160 nm injection case. Our diamond simulation is similar to the alumina simulation with injection of 160 nm monomers.

Our model evaluation of ozone impacts from alumina geoengineering considers the following reaction on bare alumina surfaces:

$$ClONO_2 + HCl \rightarrow HNO_3 + Cl_2 \qquad (R1)$$

This reaction, with reaction probability $\gamma$ of 0.02, has been studied in relation to ozone depletion resulting from space shuttle launches (Danilin et al., 2001; Jackman et al., 1998). We assume that this reaction occurs catalytically with no surface poisoning. Other potential reactions on alumina surfaces have been investigated in the laboratory (see Sander et al., 2011), and further investigation is needed to determine how additional heterogeneous and photocatalytic reactions could modify stratospheric chemistry or change the surface properties of alumina in the

Debra Weisenstein 7/27/2015 12:23 AM
**Deleted:** W

Debra Weisenstein 8/17/2015 4:31 PM
**Deleted:** emission

Debra Weisenstein 8/17/2015 4:31 PM
**Deleted:** emission

Debra Weisenstein 8/17/2015 4:31 PM
**Deleted:** emission

Debra Weisenstein 8/17/2015 4:32 PM
**Deleted:** emission

Debra Weisenstein 8/17/2015 11:43 AM
**Deleted:** , especially

stratosphere. Measurements of potential heterogeneous reactions on diamond surfaces are not available. Thus we perform diamond injection calculations assuming (R1) on diamond at the same rate as for alumina, and assuming no reactions on bare diamond surfaces.

We also consider heterogeneous reactions on the sulfate-coated surfaces of solid particles. These reactions include:

$$N_2O_5 + H_2O \rightarrow 2\ HNO_3 \quad \text{(R2)}$$

$$ClONO_2 + HCl \rightarrow HNO_3 + Cl_2 \quad \text{(R3)}$$

$$ClONO_2 + H_2O \rightarrow HNO_3 + HOCl \quad \text{(R4)}$$

$$HOCl + HCl \rightarrow H_2O + Cl_2 \quad \text{(R5)}$$

$$BrONO_2 + H_2O \rightarrow HNO_3 + HOBr \quad \text{(R6)}$$

$$BrONO_2 + HCl \rightarrow HNO_3 + BrCl \quad \text{(R7)}$$

$$HOBr + HCl \rightarrow H_2O + BrCl \quad \text{(R8)}$$

$$HOBr + HBr \rightarrow H_2O + Br_2 \quad \text{(R9)}$$

Due to the solubility of HCl, $ClONO_2$, HOCl, and HOBr in sulfuric acid solutions, reactions (R3), (R4), (R5), and (R8) can be considered bulk processes or hybrid bulk-surface processes governed by a reaction-diffusion process. For liquid spherical particles we use standard methods to calculating the reaction probability as a function of radius (Shi et al., 2001). For reactions on coated solid particles, we use the same functions, substituting the thickness of the sulfate layer in place of the radius of a spherical particle.

Calculated changes in ozone due to heterogeneous reactions on alumina surfaces (bare alumina and sulfate-coated alumina) are shown in Fig. 11 for cases with injection of 80 nm and 240 nm monomers at an injection rate of 1 Tg $yr^{-1}$. Column ozone depletion ranges from 2% in the tropics to 6-10% at midlatitudes and up to 14% at the poles in springtime with injection of 80 nm monomers. With injection of 240 nm monomers, ozone depletion is much smaller, ranging from 0.3% to 2.5%. The annual average ozone change as a function of latitude and altitude (Fig. 11, right hand panels) shows features linked to local balances in ozone's formation rate, chemical destruction rate, and local transport rates. In the tropics, ozone concentrations are determined by

Debra Weisenstein 8/17/2015 4:32 PM
**Deleted:** emission

Debra Weisenstein 7/21/2015 12:48 PM
**Deleted:** Mt yr

Debra Weisenstein 7/27/2015 11:45 AM
**Deleted:** timescale

the chemical production via UV radiation that is balanced by transport out of the tropics to higher latitudes. Thus ozone changes due to increased loss mechanisms are minimal in the tropics in the stratosphere, though increased penetration of UV to lower altitudes in the tropics can produce ozone increases. In the middle stratosphere at 25-35 km altitude, the $NO_x$ cycle dominates ozone loss. Increases in aerosol surface area density in this region reduce NO and $NO_2$ while increasing $HNO_3$ via the $N_2O_5$+$H_2O$ reaction. Thus the $NO_x$ loss cycle is diminished and ozone increases. The sedimentation rate of alumina particles is significant, as the scenario with injection of 80 nm monomers yields significant increases in aerosol surface area density and ozone changes above 25 km, whereas the scenario with 240 nm monomers injected does not. In the lower stratosphere at mid and high latitudes, the heterogeneous reactions on particle surfaces increase the ratio of chlorine and bromine in their radical forms that destroy ozone (Cl, ClO, Br, and BrO). In addition, the $N_2O_5$+$H_2O$ reaction leads to more $HNO_3$ and less $ClONO_2$ and $BrONO_2$, thus indirectly increasing halogen radicals as well. Local ozone depletions in the lower stratosphere are as large as 24% with 80 nm monomer injections and 5% with 240 nm monomer injections, on an annual average basis.

Figure 12(a) shows annual average changes in ozone column as a function of latitude with 1 Tg $yr^{-1}$ of geoengineering injections. Results with injection of 80 nm, 160 nm, and 240 nm alumina monomers are shown, along with injection of 160 nm diamond monomers. We don't calculate ozone changes due to injection of 320 nm alumina monomers because these scenarios produce less radiative forcing than injection of 240 nm monomers for similar injection rates. Ozone changes, similar to SAD increases, are found to be very sensitive to injected monomer size. However, assuming that coated alumina particles assume a more compact shape (shown by dashed lines in the figure) significantly reduces calculated ozone depletion for the $R_0$=80 nm case, and modestly reduces ozone depletion for the $R_0$=160 nm case. Also shown in Fig. 12(a) are changes in ozone column due to injection of 1 Tg $yr^{-1}$ of $SO_2$ and $H_2SO_4$, which are roughly similar to those calculated with 1 Tg $yr^{-1}$ of 80 nm alumina monomers.

Figure 12(b) shows calculated ozone changes for injection rates of 1, 2, 4, and 8 Tg $yr^{-1}$ with injection of 240 nm alumina monomers. Note than ozone changes increase at a less than linear rate with increasing injection rates, and that the effect of compaction of coated alumina particles becomes more significant at higher injection rates due to formation of higher-order fractals.

Figure 12(c) shows calculated ozone changes due to geoenginering injection of diamond

Debra Weisenstein 8/17/2015 12:47 PM
**Deleted:** ,

Debra Weisenstein 7/21/2015 12:48 PM
**Deleted:** Mt yr

Debra Weisenstein 8/17/2015 2:58 PM
**Deleted:** alumina emission

Debra Weisenstein 8/17/2015 4:33 PM
**Deleted:** emission

Debra Weisenstein 8/17/2015 2:59 PM
**Deleted:** emission

Debra Weisenstein 7/21/2015 12:48 PM
**Deleted:** Mt yr

Debra Weisenstein 8/17/2015 3:00 PM
**Deleted:** emission

Debra Weisenstein 8/17/2015 2:59 PM
**Deleted:** emission

Debra Weisenstein 8/17/2015 3:01 PM
**Deleted:** emission

monomers of 160 nm radius. Solid lines are for results including the (R1) reaction on uncoated particles, and dotted lines omit this reaction. Reaction (R1) has a greater effect in the tropics than at mid latitudes due to higher concentrations of uncoated particles there. The northern high latitudes show greater sensitivity to geoengineering injections than the southern high latitudes at the higher emission levels, likely due to the dominant role of PSCs over the Antarctic.

Global average column ozone changes are shown in Fig. 13(a) as functions of injected monomer size and injection rate. Figure 13(b) shows changes in global average ozone as a function of the associated radiative forcing for each scenario. This makes it clear that geoengineering injection of 80 nm alumina monomers is completely unworkable, producing excessive ozone depletion (5% with 1 Tg $yr^{-1}$ injection and 14% with 8 Tg $yr^{-1}$ injection) and minimal radiative forcing. Geoengineering by injection of 240 nm alumina monomers, however, could potentially be an effective climate control strategy, similar to geoengineering by injection of sulfur in its radiative forcing effectiveness but with less ozone depletion potential. Note that radiative forcing and associated ozone depletion with 16 Tg $yr^{-1}$ injection of 240 nm alumina monomers is included in the Fig. 13(b), yielding 3.6 W $m^{-2}$ of RF with about 8% ozone depletion. Injection of 160 nm diamond monomers produces ozone loss per terragram of injection similar to 160 nm alumina monomers, but with radiative forcing per terragram of injection greater than for similar injections of 240 nm alumina monomers. We show diamond results both including and excluding reaction (R1) on bare diamond surfaces. This reaction makes about a 10-15% difference in ozone depletion due to diamond injection. Note that the $SO_2$ results plotted in Fig.13 show more ozone depletion than in Heckendorn et al. (2009) because that study did not include the short-lived bromine source gases and used a narrower injection region. More studies will be needed to evaluate potential impacts on stratospheric chemistry such as tropopause heating and changes in the Brewer-Dobson circulation that are not evaluated here.

Debra Weisenstein 8/17/2015 3:01 PM
**Deleted:** emission

Debra Weisenstein 8/17/2015 3:37 PM
**Deleted:** emission

Debra Weisenstein 7/21/2015 12:48 PM
**Deleted:** Mt yr

Debra Weisenstein 7/21/2015 12:48 PM
**Deleted:** Mt yr

Debra Weisenstein 7/21/2015 12:48 PM
**Deleted:** Mt yr

Debra Weisenstein 8/17/2015 3:38 PM
**Deleted:** almost 4

Debra Weisenstein 7/24/2015 10:31 PM
**Deleted:** megaton

Debra Weisenstein 7/24/2015 10:31 PM
**Deleted:** megaton

## 4 Discussion

We have developed a new aerosol model and used it to quantitatively explore the interactions of solid particles with sulfate aerosol in the stratosphere. This analysis allows a preliminary assessment of some of the trade-offs that might arise in using solid aerosols such as alumina or

diamond rather than sulfates for solar geoengineering. We first discuss salient limitations of our model before turning to analysis of trade-offs.

### 4.1 Limitations

*Injection mechanism*. We do not model the mechanism for injection and dispersion of aerosols. If aerosols were injected from aircraft there would be small-scale dynamical effects in the injection nozzle and in the aircraft plume in which particle concentrations would be much larger than found after dilution to the scale of a model grid box, possibly leading to rapid coagulation. Effects during particle generation or injection from a nozzle would occur on very short time and space scales and cannot be estimated here. We can, however, estimate the impact of coagulation in an expanding plume using the method of Pierce et al. (2010). We allow the plume cross-section to dilute from 6 $m^2$ to $17x10^6$ $m^2$ over a 48 hours period, assuming that alumina particles are release at a rate of 30 kg $km^{-1}$ of flight path. We find the fraction of alumina mass remaining as monomers after 48 hours of plume dilution to be 37%, 86%, 96%, and 98% for injected monomers of 80, 160, 240, and 320 nm, respectively. For monomer injections of 240 and 320 nm, only 2-monomer fractals are created within 48 hours. We conclude that plume dynamics and processing are unlikely to have a substantial effect on alumina geoengineering if injected monomer size is greater than 160 nm. For 240 nm monomer, the most relevant case, our 2-D model calculation would be expected to have 4% less mass in monomers if plume dynamics were considered.

*Two-dimensional model*. A second limitation is the use of a 2-D model. Since the geoengineering scenarios discussed in this work deal with particle injection in the 20-25 km altitude region and spread between 30°S and 30°N, assuming zonal symmetry, as a 2-D model implicitly does, does not detract greatly from the validity of our results. In particular, if the method of injecting alumina particles attempts to distribute them uniformly in space and time and avoid overlapping emissions as much as possible, then a zonally-symmetric spread may be a fairly good approximation. However, details of transport near and below the tropopause are not well-represented in 2-D models. Thus a 3-D model would be needed to accurately represent this region. And if a specific geoengineering injection methodology were to be investigated, a 3-D model with fine resolution would be needed to examine heterogeneities in the resulting aerosol distribution.

*Geometry of aggregates, effects of size binning*. The fractal geometry of aggregates likely depends on the formation mechanism, and it is plausible that the actual fractal dimensions might differ significantly from the $D_f$ value of 1.6 we use here for alumina and diamond. While the fractal dimension of alumina has been measured for monomer cores much smaller than considered here, that of diamond has not. It is also plausible that variables $k_f$ and $k_h$ should have values other than 1.0, at least for cases that calculate many high-order fractals. The behavior of aggregates under stratospheric conditions has not been studied extensively. The formulations we have adopted for coagulation, condensation, and sedimentation are based on theoretical studies or on tropospheric or liquid-medium experiments, and thus should be considered uncertain. Our formulation also assumes that all injected monomers are of a uniform radius. While it appears reasonable to assume that industrial production of alumina or diamond nanoparticles could produce particles within a narrow size range, our assumption is a simplification. Likewise, our assumption of maximal compaction instantaneously on wetting is likely not realistic but meant to show the greatest possible affect of potential particle compaction on aging. Observational studies in the laboratory and in the stratosphere would be needed to determine whether compaction of alumina particles occurs and to what extent. However, compaction has a minor effect on the radiative properties and ozone depletion potential of particles with monomer sizes of ~200 nm or greater.

Debra Weisenstein 7/10/2015 4:03 PM
**Deleted:** O

Numerical errors result from the discrete aerosol size binning we employ. The discretization leads to a broadening of the size distribution during the coagulation process. Appendix A details the coagulation methodology, in which coagulation of two solid particles often leads to a new particle with size intermediate between two bins. In this case, particle mass is apportioned between two bins, leading to mass transfer into a bin larger than that of the combined new particle. This broadening of the distribution will lead to somewhat excessive sedimentation, whose error depends on the coarseness of the bin spacing. Coagulation between liquid and solid particles does not produce numerical broadening of the size distribution as the binning for mixed solid-liquid particles depends only on the size of the solid particle.

*Ozone chemistry*. The surface chemistry of alumina and other solid particles potentially useful for geoengineering has not been studied as extensively as that of sulfate particles. We include only one reaction, $ClONO_2$+HCl, on alumina and diamond particles in this modeling study. Laboratory studies have investigated some additional reactions on alumina surfaces, and there

may be others not yet explored. Reported reactions on $Al_2O_3$ surfaces include the uptake of $NO_2$ and $HNO_3$ and reactions of several volatile organic compounds, including formaldehyde, methanol, and acetic acid (Sander et al., 2011). In addition, photocatalysis reactions of several species on $Al_2O_3$ surfaces have been reported (de Richter and Caillol, 2011), and may depend on the exact composition or impurities of the particle surface. Photocatalysis of CFC compounds has been considered as a method to mitigate the atmospheric burden of greenhouse gases if augmented by artificial UV radiation in the troposphere. However, if these reactions were effective in the stratosphere, they would contribute to the formation of free radical chlorine and bromine, possibly increasing ozone depletion while reducing the lifetime the CFCs. Studies of these and other reactions under stratospheric photochemical conditions would need to be performed on any solid particle under consideration for geoengineering application.

*Missing feedbacks*. The modeling we present utilizes temperature and transport fields uncoupled from the model's chemistry and aerosols and is therefore missing a number of feedback processes that may be important in the atmosphere and may significantly change the radiative forcing or ozone depletion estimates given here. These include changes in stratospheric temperature due to aerosol heating, which would modify rates of reactions important to ozone formation and loss. Aerosol heating and enhanced equator-pole temperature gradients would also modify the strength of the Brewer-Dobson circulation and the polar vortex, with impacts on aerosol concentration, PSC formation, and ozone concentration. Increases in the temperature of the tropical tropopause layer would increase the transport of water vapor across the tropopause, increasing stratospheric $H_2O$ and OH concentrations, and reducing ozone (Heckendorn et al., 2009). These additional ozone changes would further modify stratospheric temperature and circulation. However, Heckendorn et al. (2009) found that ozone loss due to heterogeneous chemistry, without the dynamical effects of changes in temperature, water vapor, and the Brewer-Dobson strength, accounted for 75% of the ozone change.

Debra Weisenstein 7/15/2015 4:31 PM
**Deleted:**

A more uncertain feedback process is the effect of enhanced aerosol concentrations on upper tropospheric cloudiness and cloud radiative properties (Kuebbeler et al., 2012; Cirisan et al., 2013). A general circulation model with stratospheric chemistry and aerosol and cloud microphysics would be needed to evaluate these feedback effects.

## 4.2 Principal findings

Use of alumina particles for SRM is potentially useful only if the size of the injected monomers is larger than about 150 nm; the best results are only seen if the monomer radius exceeds about 200 nm. The strong dependence on monomer size can be understood if one assumes that the injection rate will be adjusted so as to produce a given radiative forcing, for example 2 W $m^{-2}$. For alumina, the peak mass-specific upscattering efficiency occurs at a radius of ~200 nm (see Fig. 6b). As the monomer size gets smaller a higher monomer density and mass injection rate is required to maintain the specified radiative forcing. The coagulation rate increases as the square of monomer density, so the fraction of monomers in aggregates increase rapidly with monomer density. Finally, the mass-specific radiative forcing for aggregates decreases quickly with the number of monomers in an aggregate (see Fig 7a), so the injection rate must be increased further to maintain a fixed radiative forcing. The net effect is that the radiative efficacy, the global radiative forcing per unit mass injection rate, declines very rapidly for particle radii below 150 nm. We find that alumina monomers with radii of roughly 240 nm provide the most radiative forcing for a given injection rate. For particle sizes beyond 240 nm, the scattering efficiency remains roughly constant while the sedimentation rate increases, contributing to a decrease in radiative forcing efficiency per unit injection rate.

As a specific example, consider the injection of 240 nm alumina monomers at a rate of 4 Tg $yr^{-1}$ evenly distributed between 30°S to 30°N and from 20-25 km in altitude. This produces a stratospheric burden of 4.6 Tg (see Fig. 5a) and global radiative forcing of 1.2 W $m^{-2}$ (see Fig. 7b). Under these conditions, coagulation of alumina particles is minimal: 81% of the alumina is in monomers and only 4% is in aggregates of more than two monomers (see Fig. 4c). Particle densities are a maximum in the lower tropical stratosphere with peak concentrations of about 4 $cm^{-3}$. The net effect of interaction with the background stratospheric sulfate is that about 50% of the stratospheric sulfate is found as a coating (Fig. 5b, right axis) with a typical depth of order 10 nm on the alumina particles. The total sulfate burden is reduced from 0.11 to 0.08 Tg (Fig. 5b, left axis) because the relatively fast fall speeds of the alumina aerosol provide a sedimentation sink for sulfates, yet the sulfate surface area density is increased by an average of 2 $\mu m^2$ $cm^{-3}$ in the lower stratosphere (Fig. 10b). The annual global average ozone column is reduced by 3.7% (Fig. 13a) with maximum ozone loss of 4 to 7% over polar regions for this scenario and the given modeling assumptions.

Debra Weisenstein 7/21/2015 12:48 PM
**Deleted:** Mt yr

Debra Weisenstein 7/21/2015 12:50 PM
**Deleted:** Mt

Debra Weisenstein 8/18/2015 9:32 PM
**Deleted:** 3

Debra Weisenstein 8/21/2015 5:17 PM
**Formatted:** Not Superscript/ Subscript

Debra Weisenstein 8/21/2015 5:20 PM
**Deleted:** 1-7

Debra Weisenstein 7/21/2015 12:50 PM
**Deleted:** Mt

Debra Weisenstein 8/21/2015 5:29 PM
**Deleted:** 1-3.5

As with sulfate aerosols, ozone concentrations increase at altitudes around 30 km in the mid stratosphere where the $NO_x$ cycle dominates but this is more than compensated by the halogen-catalyzed ozone loss in the lower stratosphere. And with injection of 240 nm monomers, sedimentation is rapid enough to preclude significant aerosol concentrations above 25-30 km. Most of the ozone impact of alumina aerosols is found to be due the increase in sulfate surface area and heterogeneous reactions on the liquid sulfuric acid. This is because most of the alumina particles are coated with sulfate at mid and high latitudes where ozone loss reactions largely determine the ozone concentration. If the rate of (R1) is set to zero in our simulations, the column ozone depletion changes by less than 15% in the extra-tropics, but up to 35% in the tropics with injection 4 Tg $yr^{-1}$ of 240 nm alumina monomers. Thus uncertainty in the rate of (R1) or the nature of the uncoated alumina surface does not have a strong influence on our calculated ozone impacts. If we assume that the alumina particle surfaces remain uncoated and that (R1) occurs on all alumina particles, we find that the ozone depletion is much less than that obtained when the surfaces do become coated, implying that (R1) on alumina surfaces has less effect on ozone than do sulfate heterogeneous reactions on the same surface area, mostly due to the effectiveness of heterogeneous bromine reactions.

We can achieve a similar radiative forcing of 1.2 W $m^{-2}$ with injection of 160 nm radius diamond monomers at 2 Tg $yr^{-1}$. This injection rate produces a stratospheric burden of 3.3 Tg of diamond. The corresponding ozone depletion due to diamond injection ranges between 3.8% globally due to increased sulfate surface area alone to 4.3% when we assume that (R1) occurs on the bare surface of diamond particles with the same reaction rate employed for alumina. However, levels of ozone depletion are highly uncertain as this reaction, and other potential heterogeneous reactions on diamond surfaces, have not been measured.

### 4.3 Comparison with sulfate aerosols

Whatever method is used to create an artificial radiative forcing, solar geoengineering is—at best—an imperfect method for reducing climate impacts. Any technology for producing radiative forcing will have a set of *technology-specific impacts*, such as ozone loss arising from the introduction of aerosol particles into the stratosphere. However the radiative forcing is produced, the *efficacy* of SRM is inherently limited by the fact that a change in solar radiative forcing

Debra Weisenstein 6/19/2015 10:08 AM
**Deleted:** This perturbation decreases column ozone by 3.6% with maximum ozone loss of 4 to 7% over polar regions.

Debra Weisenstein 8/18/2015 9:36 PM
**Deleted:** 3

Debra Weisenstein 7/21/2015 12:48 PM
**Deleted:** Mt yr

Debra Weisenstein 8/17/2015 4:33 PM
**Deleted:** emission

Debra Weisenstein 7/21/2015 12:50 PM
**Deleted:** Mt

cannot perfectly compensate for the radiative forcing caused by increasing greenhouse gases (Kravitz et al., 2014; Curry et al., 2014). A central motivation for considering solid aerosols rather than sulfates is that they might have less severe technology-specific risks. As discussed in the introduction, the principle technology-specific risks or side-effects of sulfate aerosols are ozone loss, increased diffuse light, and stratospheric heating.

Loss of stratospheric ozone and an increase in diffuse light have direct impacts on ecosystems and human health. The consequences of stratospheric heating are indirect and more speculative. Heating of the tropical tropoause layer (TTL) might be expected to increase the amount of water vapor entering the stratosphere. An increase in TTL temperature of 1 K increases the concentration of water vapor entering the stratosphere by about 0.8 ppmv (Kirk-Davidoff, 1999). Geoengineering with sulfate aerosols might heat the TTL region by several degrees, increasing stratospheric water vapor concentrations by more than 2 ppmv (Heckendorn et al., 2009). This would in turn exacerbate ozone loss and create a positive radiative forcing that would offset some of the reduction in forcing from SRM. While there is uncertainty about the exact consequences of heating the lower stratosphere, it's reasonably certain that all-else-equal, a geoengineering method that does not heat the low stratosphere is preferable to one that does.

We estimate stratospheric heating for alumina, diamond, and sulfate geoengineering scenarios with the RRTM model, as described in Section 3.4. Our results for alumina are broadly consistent with the results of Ferraro et al. (2011) for titania. Note, however, that Ross and Shaeffer (2014) conclude that the positive infrared radiative forcing from alumina can be larger than the negative radiative forcing from solar scattering by the same particles. We suspect that part of this discrepancy comes from the fact that Ferraro et al. (2011) and this paper assume a narrow size distribution close to the optimal for solar scattering, whereas Ross and Shaeffer (2004) use a broad alumina size distribution. However, we have not resolve this discrepancy, so our estimate of heating for alumina should be taken as uncertain.

As shown in Table 2, our results suggest that alumina may have less severe technology-specific risks than sulfates. While the injected mass necessary to achieve a -2 W $m^{-2}$ radiative forcing is roughly equivalent whether employing alumina or sulfate aerosol, the ozone depletion is more severe with sulfate geoengineering. In addition, the increase in diffuse solar radiation would be half as much with alumina as with sulfate, and the stratospheric heating is expected to be

Debra Weisenstein 5/26/2015 5:45 PM
**Deleted:** 1

considerably less, smaller by a factor of 4-5 in our estimation. Diamond appears to offer excellent shortwave scattering with only a small increase in diffuse light. We estimate ozone depletion due to diamond to be less than that due to sulfate, but uncertainty is large. Lower stratospheric heating from diamond is quite small.

We conclude that SRM by injection of solid particles may have some advantages relative to sulfates and merits further study to reduce the sizable uncertainties that currently exist. It is important to note that the injection of substances like alumina or diamond nanoparticles have much greater "unknown unknowns" than sulfates, as they would be novel substances in the stratosphere. Laboratory studies of reaction kinetics for these particles under stratospheric conditions, as well as studies of their microphysical and radiative properties, are required to reduce uncertainties.

Debra Weisenstein 8/20/2015 2:26 PM
**Deleted:** Longwave

Debra Weisenstein 8/20/2015 2:27 PM
**Deleted:** absorption

Debra Weisenstein 8/20/2015 2:27 PM
**Deleted:** insignificant

## Appendix A: Microphysical schemes for coagulation and condensation

### A.1 Coagulation

#### A.1.1 Coagulation between particles of similar composition

In our sectional aerosol representation, collisions between particles of similar composition in bins i and j, where bin j is smaller than bin i, produce particles of size intermediate between bins i and i+1. Since the volume ratio between size bins, $V_{rat}$, is 2.0 in our case, coagulation between two particles in bin i yields one particle in bin i+1. The rate of coagulation between particles in bin i and particles in bin j, $\beta_{ij}$, is a function of the coagulation kernel, $K_{ij}$, and the number densities of the particles in each bin, $N_i$ and $N_j$.

$$\beta_{ij} = SN_jN_iK_{ij}$$

where S=0.5 if i= j, otherwise S=1.0. A coagulation event between a particle in bin i and a particle in bin j ($j \leq i$) changes particle number densities in three bins as follows:

$$\frac{dN_j}{dt} = -\beta_{ij}$$

$$\frac{dN_i}{dt} = -\beta_{ij}\frac{F}{(V_{rat}-1)}$$

$$\frac{dN_{i+1}}{dt} = +\beta_{ij}\frac{F}{(V_{rat}-1)}$$

where $F = \frac{V_j}{V_i}$.

Coagulation of sulfate particles with other sulfate particles and of alumina particles with other alumina particles is generated by a double sum of the above equations over all bins i and j, where $j \leq i$. Our explicit formulation generates $\frac{dN}{dt}$ for all size bins before updating any values of N.

A.1.2 Coagulation between sulfate particles and solid particles

Coagulation between pure sulfate particles and pure alumina particles transfers particles from the category of pure alumina to the category of coated alumina, and shifts sulfate mass from pure sulfate particles to coated alumina sulfate mass. Since coated alumina particles are binned by their alumina mass alone, the alumina size index is unchanged in this coagulation process. For coagulations between an alumina particle of bin i and a sulfate particle of bin j, the rate of change of concentrations is:

$$\frac{dN_j(S)}{dt} = -\beta_{ij}$$

$$\frac{dN_i(Al)}{dt} = -\beta_{ij}$$

$$\frac{dN_i(c\text{-}Al)}{dt} = +\beta_{ij}$$

$$\frac{dM_i(S\text{-}Al)}{dt} = +\beta_{ij}\,DS_j$$

where N(S), N(Al), N(c-Al) represent number concentrations of pure sulfate, pure alumina, and coated alumina particles, respectively, M(S-Al) represents the mass of sulfate on a coated alumina particle, and $DS_j$ represents the mass of sulfate in a single pure sulfate particle of bin j. Coagulation between a pure sulfate particle of bin j and a coated alumina particle of bin i removes a sulfate particle and transfers its sulfate mass onto the coated alumina particle:

$$\frac{dN_j(S)}{dt} = -\beta_{ij}$$

$$\frac{dM_i(S-Al)}{dt} = +\beta_{ij}\, DS_j$$

A.1.3 Coagulation between different types of solid particles

For coagulation between an uncoated and a coated alumina particle:

$$\frac{dN_j(Al)}{dt} = -\beta_{ij}$$

$$\frac{dN_i(c-Al)}{dt} = -\beta_{ij}\frac{F}{(V_{rat}-1)}$$

$$\frac{dN_{i+1}(c-Al)}{dt} = +\beta_{ij}\frac{F}{(V_{rat}-1)}$$

$$\frac{dM_i(S-Al)}{dt} = -\beta_{ij}\frac{F}{(V_{rat}-1)}\, DSAl_i$$

$$\frac{dM_{i+1}(S-Al)}{dt} = +\beta_{ij}\frac{F}{(V_{rat}-1)}\, DSAl_i$$

where $DSAl_i$ represents the mass of sulfate on a single coated alumina particle of bin i, obtained as the ratio of total sulfate mass on solid particles of bin i for a given grid box to the number of coated alumina particles in that grid box.

For coagulation between two coated alumina particles:

$$\frac{dN_j(c-Al)}{dt} = -\beta_{ij}$$

$$\frac{dN_i(c-Al)}{dt} = -\beta_{ij}\frac{F}{(V_{rat}-1)}$$

$$\frac{dN_{i+1}(c-Al)}{dt} = +\beta_{ij}\frac{F}{(V_{rat}-1)}$$

$$\frac{dM_j(S-Al)}{dt} = -\beta_{ij}\, DSAl_j$$

$$\frac{dM_i(S-Al)}{dt} = -\beta_{ij}\, DSAl_i + \beta_{ij}\left(1-\frac{F}{(V_{rat}-1)}\right)(DSAl_j + DSAl_i)$$

$$\frac{dM_{i+1}(S-Al)}{dt} = +\beta_{ij}\ \frac{F}{(V_{rat}-1)}\ (DSAl_j + DSAl_i)$$

A.1.4 Coagulation kernel

The coagulation kernels, $K_{ij}$, are calculated following classical theory as detailed in Jacobson (1999). We apply only Brownian coagulation without convective, gravitational, or Van der Waals corrections.

$$K_{ij} = \frac{4\pi(r_i + r_j)(D_i + D_j)}{\frac{r_i+r_j}{r_i+r_j+(\delta_i^2+\delta_j^2)^{1/2}} + \frac{4(D_i+D_j)}{(r_i+r_j)(\bar{c}_i^2+\bar{c}_j^2)^{1/2}}}$$

$$\delta_i = \frac{(2r_i + \lambda_i)^3 - (4r_i^2 + \lambda_i^2)^{3/2}}{6r_i\lambda_i} - 2r_i$$

where $r_i$ represents particle radius, $D_i$ represents the particle diffusion coefficient, $\bar{c}_i$ represents the thermal velocity of the particle, and $\lambda_i$ represents the particle mean free path.

For liquid particles, we use the spherical radius in the calculation of coagulation kernels; for solid particles we use the radius of gyration $R_g$ in the calculation (Maricq, 2007), as this more closely represents the distance over which fractal particles may interact with other particles.

A.2 Condensational Growth and Evaporation

The rate of $H_2SO_4$ vapor condensation onto sulfate particles or sulfate-coated alumina particles of bin *i* follows Jacobson (1999) and is given by:

$$\frac{dN_{H2SO4}}{dt} = \frac{-S_i\, N_i\, D_v\, \left(N_{H2SO4} - \alpha N_{H2SO4}^{eq}\right)}{r_i}$$

where $S_i$ represents the surface area of a single particle in bin *i*, $N_i$ the particle number density, $D_v$ is the molecular diffusion coefficient of the $H_2SO_4$ vapor, $N_{H2SO4}$ represents the number density of ambient $H_2SO_4$ gas, and $N_{H2SO4}^{eq}$ the equilibrium $H_2SO_4$ number density above a liquid $H_2SO_4$ surface. $\alpha$ is the Kelvin effect correction term, representing the saturation vapor pressure over a curved surface relative to that over a flat surface, given by:

$$\alpha = \exp\left(\frac{2\sigma_p\mu_p}{r_i R^* T \rho_p}\right).$$

$\alpha$ is a function of the surface tension of the $H_2SO_4$ liquid, $\sigma_p$, the average molecular weight of the liquid, $\mu_p$, the particle radius, $r_i$, gas constant R*, temperature, T, and liquid solution density $\rho_p$. The diffusion coefficient is defined as:

$$D_v = \frac{3}{8d^2 N_{air}} \left( \frac{k_B T A_V}{2\pi \mu_{H2SO4}} \frac{\mu_{air} + \mu_{H2SO4}}{\mu_{air}} \right)^{0.5} \omega$$

$$\omega = \left\{ 1 + \left[ \frac{1.3333 + 0.71 K_n^{-1}}{1 + K_n^{-1}} \right] K_n \right\}^{-1}$$

where d is the diameter of a gas molecule, $k_B$ is Boltzman's constant, and $A_v$ is Avogadro's number, $\omega$ is a correction term for collision geometry, and $K_n$ is the Knudsen number. We assume an accommodation coefficient of 1.0. We use the spherical radius in the calculations for pure sulfuric acid-water particles, and the radius of gyration, $R_g$, increased by the coating thickness, for the sulfate-coated solid particles. However, for the curvature term $\alpha$, we use the radius of the monomers composing the fractal particles increased by the coating thickness. The particle surface area for fractal particles is as described in Section 2 of this paper.

In the case of pure liquid $H_2SO_4$-$H_2O$ particles, condensation increases the particle radius and shifts mass into larger size bins, much as the coagulation formulation described above distributes mass between two bins when a particle's radius would fall between two bins. For sulfate-coated alumina particles, the bin is defined by the radius of the alumina particle only, so the size bin remains constant while the mass of sulfate associated with that bin increases. Evaporation occurs via the identical equations when $N_{H2SO4}$ is less than $\alpha N_{H2SO4}^{eq}$ and $\frac{dN_{H2SO4}}{dt}$ becomes positive. This occurs above about 35 km for sulfuric acid particles.

Debra Weisenstein 7/13/2015 12:25 PM
**Deleted:** exp

## Author contributions

D. Keith conceived this study and provided overall scientific direction. D. Weisenstein developed the solid-liquid aerosol model and performed the 2-D calculations. D. Keith performed the SW radiative forcing calculations, while J. Dykema calculated the heating rates with LW and SW contributions.

Debra Weisenstein 8/25/2015 10:35 AM
**Deleted:** ,

Debra Weisenstein 8/25/2015 10:35 AM
**Deleted:** while

Debra Weisenstein 8/25/2015 10:37 AM
**Deleted:** shortwave

Debra Weisenstein 8/25/2015 10:47 AM
**Deleted:** Both authors contributed substantially to manuscript preparation.

## Acknowledgements

Funding for this study provided by a grant from the Fund for Innovative Climate and Energy Research (FICER). The authors would like to thank Frank Keutsch and Sebastian Eastham for insightful comments on earlier drafts of this paper. The authors would also like to thank two anonymous reviewers for constructive suggestions which have improved this paper.

Debra Weisenstein 8/24/2015 3:42 PM
**Deleted:**

Debra Weisenstein 8/25/2015 9:13 AM
**Deleted:** John Dykema for assistance with longwave heating calculations, and

## References

Anderson, S. B., Weatherhead, E. C., Stevermer, A., Austin, J., Brühl, C., Fleming, E. L., de Grandpre, J., Grewe, V., Isaksen, I., Pitari, G., Portmann, R. W., Rognerud, B., Rosenfield, J. E., Smyshlyaev, S., Nagashima, T., Velders, G. J. M., Weisenstein, D. K., and Xia, J.: Comparison of recent modeled and observed trends in total column ozone, J. Geophys. Res., 111, D02303, doi:10.1029/2005JD006091, 2006.

Blackstock, J. J., Battisti, D. S., Caldeira, K., Eardley, D. M., Katz, J. I., Keith, D. W., Patrinos, A. A. N., Schrag, D. P., Socolow, R. H., and Koonin, S. E.: Climate Engineering Responses to Climate Emergencies. Novim, available at: http://arxiv.org/ pdf/0907.5140, 2009.

Bohren, C. F., and Huffman, D. R.: Absorption and scattering of light by small particles. John Wiley & Sons, 2008.

Brock, C. A., Hamill, P., Wilson, J. C., Jonsson, H. H., Chang, K. R.: Particle formation in the upper tropical troposphere: A source of nuclei for the stratospheric aerosol, Science, 270, 1650-1653, 1995.

Charlson, R. J., Langner, J., Rodhe, H., Leovy, C. B., and Warren, S. G.: Perturbation of the northern hemisphere radiative balance by backscattering from anthropogenic sulfate aerosols, Tellus A, 43, 152-163, 1991.

Cirisan, A., Spichtinger, P., Luo, B. P., Weisenstein, D. K., Wernli, H., Lohmann, U., and Peter, T.: Microphysical and radiative changes in cirrus clouds by geoengineering the stratosphere, J. Geophys. Res., 118, 4533-4548, doi:10.1002/jgrd.50388, 2013.

Clough, S. A., Shephard, M. W., Mlawer, E. J., Delamere, J. S., Iacono, M. J., Cady-Pereira, K., Boukabara, S., Brown, P. D.: Atmospheric radiative transfer modeling: a summary of the AER

codes, J. Quant. Spectrosc. Radiat. Transfer., 91, 233-244, 2005.

Curry, C. L., Sillmann, J., Bronaugh, D., Alterskjaer, K., Cole, J. N. S., Ji, D., Kravitz, B., Kristjansson, J. E., Moore, J. C., Muri, H., Niemeier, U., Robock, A., Tilmes, S., and Yang, S.: A multimodel examination of climate extremes in an idealized geoengineering experiment, J. Geophys. Res., 119, 3900-3923, doi:10.1002/2013JD020648, 2014.

Danilin, M. Y., Shia, R.-L., Ko, M. K. W., Weisenstein, D. K., Sze, N. D., Lamb, J. J., Smith, T. W., Lohn, P. D., and Prather, M. J.: Global stratospheric effects of the alumina emissions by solid-fueled rocket motors, J. Geophys. Res., 106, 12,727-12,738, 2001.

De Richter, R., and Caillol, S.: Fighting global warming: The potential of photocatalysis against $CO_2$, $CH_4$, $N_2O$, CFCs, tropospheric $O_3$, BC and other major contributors to climate change, J. Photochem. and Photobio. C: Photochemistry Reviews, 12, 1-19, doi:10.1016/j.jphotochemrev.2011.05.002, 2011.

Dvortsov, V. L., Geller, M. A., Yudin, V. A., and Smyshlyaev, S. P.: Parameterization of the convective transport in a two-dimensional chemistry-transport model and its validation with radon 222 and other tracer simulations, J. Geophys. Res., 103, 22047–22062, doi:10.1029/98JD02084, 1998.

Edwards, D. F., and Philipp, H. R.: "Cubic carbon (diamond)" in Handbook of Optical Constants of Solids, ed. E. Palik, Academic Press Inc., San Diego, CA, USA, 1985.

English, J. M., Toon, O. B., and Mills, M. J.: Microphysical simulations of sulfur burdens from stratospheric sulfur geoengineering, Atmos. Phys. Chem., 12, 4775-4793, doi:10.5194/acp-12-4775-2012, 2012.

Ferraro, A. J., Highwood, E. J., and Charlton-Oerez, A. J.: Stratospheric heating by potential geoengineering aerosols, Geophys. Res. Lett., 38, L24706, doi:10.10292011GL049761, 2011.

Fleming, E. L., Jackman, C. H., Stolarski, R. S., and Considine, D. B.: Simulation of stratospheric tracers using an improved empirically-based two-dimensional model transport formulation, J. Geophys. Res., 104, 23,911-23,934, 1999.

Filippov, A. V., Zurita, M., and Rosner, D. E.: Fractal-like aggregates: Relation between morphology and physical properties, J. Colloid Interf. Sci., 229, 261-273, 2000.

Hamill, P., Jensen, E. J., Russell, P, B., and Bauman, J. J.: The life cycle of stratospheric aerosol particles, B. Am. Meteor. Soc., 78, 1395-1410, 1997.

Hanson, D., and Mauersberger, K.: Laboratory studies of the nitric acid trihydrate: Implications for the south polar stratosphere, Geophys. Res. Lett. 15, 855-858, 1988.

Heckendorn, P., Weisenstein, D., Fueglistaler, S., Luo, B. P., Rozanov, E., Schraner, M., Thomason, L. W., and Peter, T.: The impact of geoengineering aerosols on stratospheric temperature and ozone, Environ. Res. Lett., 4, 045108, doi:10.1088/1748-9326/4/4/045108, 2009.

Hinklin, T., Toury, B., Gervais, C., Babonneau, F., Gislason, J. J., Morton, R. W., and Laine, R. M.: Liquid-feed flame spray pyrolysis of metalloorganic and inorganic alumina sources in the production of nanoalumina powders, Chem. Mater., 16, 21-30, doi:10.1021/cm021782t, 2004.

Jackman, C. H., Considine, D. B., and Fleming, E. L.: A global modeling study of solid rocket aluminum oxide emission effects on stratospheric ozone, Geophys. Res. Lett., 25, 907-910, 1998.

Jacobson, M. Z.: Fundamentals of Atmospheric Modeling, Cambridge University Press, 1999.

Johnson, C. P., Li, X., and Logan, B. E.: Settling velocities of fractal aggregates, Environ. Sci. Technol., 30, 1911-1918, 1996.

Kajino, M., and Kondo, Y.: EMTACS: Development and regional-scale simulation of a size, chemical, mixing type, and soot shape resolved atmospheric particle model, J. Geophys. Res., 116, D02303, doi:10.1029/2010JD015030, 2011.

Karasev, V. V., Onishchuk, A. A., Glotov, O. G., Baklinov, A. M., Zarko, V. E., and Panfilov, V. N.: Charges and fractal properties of nanoparticles – Combusion products of aluminum agglomerates, Combust. Explo. Shock+, 37, 734-736, 2001.

Karasev, V. V., Onischuk, A. A., Glotov, O. G., Baklanov, A. M., Maryasov, A. G., Zarko, V. E., Panfilov, V. N, Levykin, A. I., and Sabelfeld, K. K.: Formation of charged aggregates of $Al_2O_3$ nanoparticles by combustion of aluminum droplets in air, Combust. Flame, 138, 40-54, 2004.

Keith, D. W.: Photophoretic levitation of engineered aerosols for geoengineering, Proc. Natl. Acad. Sci. USA, 107, 16428–16431, doi: 10.1073/pnas.1009519107, 2010.

Kirk-Davidoff, D. B, Hintsa, E. J., Anderson, J. G., and Keith, D. W.: The effect of climate change on ozone depletion through changes in stratospheric water vapour, Nature, 402, 399-401, 1999

Kravitz, B., MacMartin, D. G., and Caldeira, K.: Geoengineering: Whiter skies? Geophys. Res. Lett., 39, L11801, doi:10.1029/2012GL051652, 2012.

Kravitz, B., MacMartin, D. G., Robock, A., Rasch, P. J., Ricke, K. L., Cole, J. N. S., Curry, C. L., Irvine, P. J., Ji, D., Keith, D. W., Kristjansson, J. E., Moore, J. C., Muri, H., Singh, B., Tilmes, S., Watanabe, S., Yang, S., and Yoon, J.-H.: A multi-model assessment of regional climate disparities caused by solar geoengineering, Environ. Res. Lett., 9, 074013, doi:10.1088/1748-9326/9/7/074013, 2014.

Krueger, A.: Diamond nanoparticles: Jewels for chemistry and physics, Adv. Mater., 20, 2445-2449, doi:10.1002/adma.200701856, 2008.

Kuebbeler, M., Lohmann, U., and Feichter, J.: Effects of stratospheric sulfate aerosol geo-engineering on cirrus clouds, Geophys. Res. Lett., 39, L23803, doi:10.1029/2012GL053797, 2012.

Lawrence, C. R., and Neff, J. C.: The contemporary physical and chemical flux of aeolian dust: A synthesis of direct measurements of dust deposition, Chem. Geol., 267, 46063, doi:10.1016/j.chemgeo.2009.02.005, 2009.

Maricq, M. M.: Coagulation dynamics of fractal-like soot aggregates, J. Aerosol Sci., 38, 141-156, 2007.

Maricq, M. M., and Nu, N.: The effective density and fractal dimension of soot particles from premixed flames and motor vehicle exhaust, J. Aerosol Sci., 35, 1251-1274, 2004.

Marti, J., and Mauersberger, K.: A survey and new measurements of ice vapor pressure at temperatures between 170 and 250K, Geophys. Res. Lett. 20, 363-366, 1993.

McClellan, J., Keith, D. W., and Apt, J.: Cost analysis of stratospheric albedo modification delivery systems, Environ. Res. Lett., 7, 034019, doi: 10.1088/1748-9326/7/3/034019, 2012.

Mercado, L. M., Bellouin, N., Sitch, S., Boucher, O., Huntiongford, C., Wild, M., and Cox, P. M.: Impact of changes in diffuse radiation on the global land carbon sink, Nature, 458, 1014-1018, doi:10.1038/nature07949, 2009,

Mikhailov, E. F., Vlasenko, S. S., Podgorny, I. A., Ramanathan, V., and Corrigan, C. E.: Optical properties of soot-water drop agglomerates: An experimental study, J. Geophys. Res., 111, D07209, doi:10.1029/2005JD006389, 2006.

Mlawer, E. J., Taubman, S. J, Brown, P. D., Iacono, M. J., and Clough, S. A.: RRTM, a validated correlated-k model for the longwave. J. Geophys. Res., 102, 16,663-16,682, 1997.

Molina, M. J., Molina, L. T., Zhang, R., Meads, R. F., and Spencer, D. D.: The reaction of $ClONO_2$ with HCl on aluminum oxide, Geophys. Res. Lett., 24, 1619-1622, doi:10.1029/97GL01560, 1997.

Moreno-Cruz, J., Ricke, K., and Keith, D. W.: A simple model to account for regional inequalities in the effectiveness of solar radiation management. Climatic Change, 110, 649-668. doi:10.1007/s10584-011-0103-z, 2011.

Niemeier, U., Schmidt, H., and Timmreck, C.: The dependency of geoengineered sulfate aerosol on the emission strategy, Atmos. Sci. Lett., 12, 189-194, doi:10.1002/asl.304, 2011.

Pierce, J. R., Weisenstein, D. K., Heckendorn, P., Peter, T., and Keith, D. W.: Efficient formation of stratospheric aerosol for climate engineering by emission of condensible vapor from aircraft, Geophys. Res. Lett., 37, L18805, doi:10.1029/2010GL043975, 2010.

Pitari, G., Aquila, V., Kravitz, B., Robock, A., Watanabe, S., Cionni, I., De Luca, N., Di Genova, G., Mancini, E., and Tilmes, S.: Stratospheric ozone response to sulfate geoengineering: Results from the Geoengineering Model Intercomparison Project (GeoMIP), J. Geophys. Res., 119, 2629-2653, doi:10.1002/2013JD020566, 2014.

Pope, F. D., Braesicke, P., Grainger, R. G., Kalberer, M., Watson, I. M., Davidson, P. J., and Cox, R. A.: Stratospheric aerosol particles and solar-radiation management, Nature Climate Change, 2, 713-719, doi:10.1038/NCLIMATE1528, 2012.

Rannou, P., McKay, C. P., Botet, R., and Cabane, M.: Semi-empirical model of absorption and scattering by isotropic fractal aggregates of spheres, Planet. Space Science, 47, 385-396, 1999.

Rasch, P. J., Crutzen, P. J., Coleman, D. B.: Exploring the geoengineering oc climate using stratospheric sulfate aerosols: the role of particle size, Geophys. Res. Lett., 35, L02809, doi:10.1029/2007GL032179, 2008.

Rinsland, C. P., Weisenstein, D. K., Ko, M. K. W., Scott, C. J., Chiou, L. S., Mahieu, E., Zander, R., and Demoulin, P.: Post-Mount Pinatubo eruption ground-based infrared stratospheric column measurements of $HNO_3$, NO, and $NO_2$ and their comparison with model calculations, J. Geophys. Res., 108, 4437, doi:10.1029/2002JD002965, 2003.

Ross, M. N., and Shaeffer, P. M.: Radiative forcing caused by rocket engine emissions, Earth's Future, 2, 177-196, doi:10.1002/2013EF000160, 2014.

Sander, S. P., Friedl, R. R., Barker, J. R., Golden, D. M., Kurylo, M. J., Wine, P. H., Abbatt, J. P. D., Burkholder, J. B., Kolb, C. E., Moortgat, G. K., Huie, R. E.: Chemical kinetics and photochemical data for use in atmospheric studies, Evaluation No. 17, JPL Publication 10-6, 2011.

Seinfeld, J. H., and Pandis, S. N.: Atmospheric Chemistry and Physics, John Wiley and Sons, Inc., 2006.

Shi, Q., Jayne, J. T., Kolb, C. E., Worsnop, D. R., and Davidovits, P.: Kinetic model for reaction of $ClONO_2$ with $H_2O$ and HCl and HOCl with HCl in sulfuric acid solutions, J. Geophys. Res., 106, 24,259-24,274, 2001.

Shrand, A. M., Huang, H., Carlson, C., Schlager, J. J., Osawa, E., Hussain, S. M., and Dai, L.: Are diamond nanoparticles cytotoxic? J. Phys Chem. B, 111, 2-7, doi:10.1021/jp066387v, 2007.

Solomon, S.: Stratospheric ozone depletion: a review of concepts and history, Rev. Geophys., 37, 275-316, doi:10.1029/1999RG900008, 1999.

SPARC: SPARC Report No. 4, Assessment of Stratospheric Aerosol Properties (ASAP), WCRP-124 WMO/TD No. 1295, SPARC Report No. 4, edited by L. Thomason and Th. Peter, WMO, 2006.

Stamnes, K., Tsay, S. C., Wiscombe, W., and Jayaweera, K.: Numerically stable algorithm for discrete-ordinate-method radiative transfer in multiple scattering and emitting layered media, App. Opt., 27, 2502-2509, 1988.

Debra Weisenstein 6/24/2015 1:44 PM
**Moved down [1]:** Shrand, A. M., Huang, H., Carlson, C., Schlager, J. J., Osawa, E., Hussain, S. M., and Dai, L.: Are diamond nanoparticles cytotoxic? J. Phys Chem. B, 111, 2-7, doi:10.1021/jp066387v, 2007.

Debra Weisenstein 6/24/2015 1:44 PM
**Moved (insertion) [1]**

Tabazadeh, A., Toon, O. B., Cleg, S. L., and Hamill, P.: A new parameterization of $H_2SO_4/H_2O$ aerosol composition: Atmospheric implications, Geophys. Res., Lett., 24, 1931–1934, 1997.

Tang, M. J., Camp, J. C. J., Rkiouak, L., McGregor, J., Watson, I. M., Cox, R. A., Kalberer, M., Ward, A. D., and Pope, F. D.: Heterogeneous Interaction of $SiO_2$ with $N_2O_5$: Aerosol Flow Tube and Single Particle Optical Levitation-Raman Spectroscopy Studies, J. Phys. Chem. A, 118, 8817-8827, 2014a.

Tang, M. J., Telford, P. J., Pope, F. D., Rkiouak, L., Abraham, N. L., Archibald, A. T., Braesicke, P., Pyle, J. A., McGregor, J., Watson, I. M., Cox, R. A., and Kalberer, M.: Heterogeneous reaction of $N_2O_5$ with airborne $TiO_2$ particles and its implication for stratospheric particle injection, Atmos. Chem. Phys., 14, 6035-6048, 2014b.

Teller, E., Wood, L., and Hyde, R.: Global Warming and Ice Ages: I. Prospects for Physics-Based Modulation of Global Change, Lawrence Livermore National Laboratory Publication UCRL-JC-128715, 18 pp., 1997.

Tilmes, S., Muller, R., and Salawitch, R.: The sensitivity of polar ozone depletion to proposed geoengineering schemes, *Science, 320*, 1201-1204, DOI: 10.1126/science.1153966, 2008.

Tilmes, S., Garcia, R. R., Kinnison, D. E., Gettelman, A., and Rasch, P. J.: Impact of geoengineered aerosols on the troposphere and stratosphere, J. Geophys. Res., 114, D12305, doi:10.1029/2008JD011420, 2009.

Tilmes, S., Kinnison, D. E., Garcia, R. R., Salawitch, R., Canty, T., Lee-Taylor, J., Madronich, S., and Chance, K.: Impact of very short-lived halogens on stratospheric ozone abundance and UV radiation in a geo-engineered atmosphere, Atmos. Chem. Phys., 12, 10945-10955, doi:10.5194/acp-12-10945-2012, 2012.

Thomas, M. E., and Tropf, W. J.: "Aluminum Oxide ($Al_2O_3$) Revisited" in Handbook of Optical Constants of Solids, Vol. 3, ed. Palik, Edward D., Academic Press Inc., St. Louis, MO, USA, 1997

Tsuzuki, T., and McCormick, P. G.: Mechanochemical synthesis of nano particles, J. Materials Sci., 39, 5143-5146, 2004.

U.S. Geological Survey (USGS): 2012 Minerals Yearbook: Bauxite and Alumina, U.S. Department of the Interior, Washington, D.C., http://minerals.usgs.gov/minerals/pubs/commodity/bauxite/myb1-2012-bauxi.pdf , May 2014.

Weisenstein, D. K., Yue, G. K., Ko, M. K. W., Sze, N.-D., Rodriguez, J. M., and Scott, C. J.: A two-dimensional model of sulfur species and aerosols, J. Geophys. Res., 102, 13,019-13,035, 1997.

Weisenstein, D. K., Ko, M. K. W., Dyominov, I. G., Pitari, G., Picciardulli, L., Visconti, G., and Bekki, S.: The effects of sulfur emission from HSCT aircraft: A 2-D model intercomparison, J. Geophys. Res., 103, 1527-1547, 1998.

Weisenstein, D. K., Eluszkiewicz, J., Ko, M. K. W., Scott, C. J, Jackman, C. H., Fleming, E. L., Considine, D. B., Kinnison, D. E., Connell, P. S., and Rotman, D. A.: Separating chemistry and transport effects in 2-D models, J. Geophys. Res., 109, D18310, doi:10.1029/2004JD004744, 2004.

Weisenstein, D. K., Penner, J. E., Herzog, M., and Liu, X.: Global 2-D intercomparison of sectional and modal aerosol modules, Atmos. Chem. Phys., 9, 2339-2355, 2007.

Wilton, D. J., Hewett, C. N., and Beerling, D. J.: Simulated effects of changes in direct and diffuse radiation on canopy scale isoprene emissions from vegetation following volcanic eruptions, Atmos. Chem. Phys., 11, 11723-11731, doi:10.5194/acp-11-11723-2011, 2011.

Wiscombe, W. J., and Grams, G. W.: The backscattered fraction in two-stream approximations, J. Atmos. Sci., 33, 2440-2451, 1976.

Table 1. Overview of experiments performed with the AER 2-D model.

| Substance Injected | Injected Particle Radius | Injection Rate (Tg $yr^{-1}$) | Fractal Dimension $D_f$ | Comments |
|---|---|---|---|---|
| Alumina | $R_0$ = 80 nm[a] | 1, 2, 4, 8 | 1.6, 2.8 | |
| Alumina | $R_0$ = 160 nm[a] | 1, 2, 4, 8 | 1.6, 2.8 | |
| Alumina | $R_0$ = 240 nm[a] | 1, 2, 4, 8, 16 | 1.6, 2.8 | |
| Alumina | $R_0$ = 320 nm[a] | 1, 2, 4, 8 | 1.6, 2.8 | |
| Diamond | $R_0$ = 160 nm[a] | 1, 2, 4, 8 | 1.6 | |
| $SO_2$ | Gas phase | 1, 2, 4, 10[c] | | Replication of Pierce et al. (2010) |
| $H_2SO_4$ | $R_g$ = 95 nm, $\sigma$ = 1.5[b] | 1, 3, 6, 15[c] | | Replication of Pierce et al. (2010) |

[a] monomers of uniform radius

[b] lognormal distribution defined by mode radius, $R_g$, and width, $\sigma$, representing distribution after plume processing

[c] based on molecular weight of $SO_2$ or $H_2SO_4$, not S alone.

Table 2. Comparison of alumina, diamond, and sulfate solar geoengineering, based on a top-of-atmosphere shortwave radiative forcing of -2 W $m^{-2}$ for each case.

| Metric | Alumina 240 nm | Diamond 160 nm | Sulfate as $H_2SO_4$ | Sulfate as $SO_2$ | Comments |
|---|---|---|---|---|---|
| SW Radiative forcing per unit injected mass flux (W $m^{-2}$ (Tg $yr^{-1}$)$^{-1}$) | -0.26 | -0.42 | -0.25[a] | -0.20[a] | Other than diamond, the differences are minor. |
| Ozone impact (global average column change) | -5.6% | -6.1% to -7.1%[b] | -13%[c] | -11%[c] | Alumina and diamond have less ozone depletion than sulfates, though there is considerable uncertainty. |
| Diffuse light increase (W $m^{-2}$) | 10.1 | 6.3 | 21 | 19 | Alumina and diamond are both better (less diffuse light) than sulfates. Exact results would require a more sophisticated radiative transfer model. |
| Heating rate (K $day^{-1}$) in tropical lower stratosphere | 0.052-0.060[d] | 0.007-0.010[d] | 0.22 | 0.30 | Alumina is probably better (less heating) than sulfates, but this estimate is subject to considerable uncertainty. Diamond is much better. |

[a] Sulfate emission fluxes based on mass of $H_2SO_4$ or $SO_2$ injected annually.

[b] The results for diamond are a range based on two cases, with and without reaction (R1) occurring on bare diamond surfaces.

[c] Note that the overall ozone loss from $H_2SO_4$ and $SO_2$ injection is higher than reported in most previous studies because we consider short-lived bromine species

Debra Weisenstein 5/22/2015 2:46 PM
**Deleted:** 1
Debra Weisenstein 7/29/2015 8:39 PM
**Deleted:** 9
Debra Weisenstein 7/29/2015 8:39 PM
**Deleted:** 50
Debra Weisenstein 7/30/2015 12:44 AM
**Deleted:** 9
Debra Weisenstein 7/30/2015 8:45 AM
**Deleted:** 22
Debra Weisenstein 7/21/2015 12:48 PM
**Deleted:** Mt yr
Debra Weisenstein 7/29/2015 11:03 PM
**Deleted:** 6
Debra Weisenstein 7/30/2015 12:49 AM
**Deleted:** 3
Debra Weisenstein 8/20/2015 3:14 PM
**Deleted:**
Debra Weisenstein 7/30/2015 12:47 AM
**Deleted:** 0
Debra Weisenstein 8/20/2015 3:14 PM
**Deleted:**
Debra Weisenstein 8/20/2015 3:14 PM
**Deleted:**
Debra Weisenstein 7/29/2015 10:53 PM
**Deleted:** 9.2
Debra Weisenstein 7/29/2015 10:51 PM
**Deleted:** 5.7
Debra Weisenstein 7/30/2015 12:42 AM
**Deleted:** 18
Debra Weisenstein 7/30/2015 12:39 AM
**Deleted:** 6
Debra Weisenstein 8/19/2015 4:37 PM
**Deleted:** 0.03
Debra Weisenstein 7/29/2015 10:59 PM
**Deleted:** <0.00
Debra Weisenstein 8/11/2015 7:24 PM
**Deleted:** 16
Debra Weisenstein 8/13/2015 2:29 PM
**Deleted:** 13
Debra Weisenstein 7/29/2015 10:57 PM
**Deleted:** 3
Debra Weisenstein 7/29/2015 10:59 PM
**Deleted:** 1
Debra Weisenstein 7/29/2015 10:55 PM
**Deleted:** and
Debra Weisenstein 6/19/2015 8:49 AM
**Deleted:** emit

[d] The range for alumina and diamond is based on average particle number densities of monomers and of total particles.

## Figure Captions

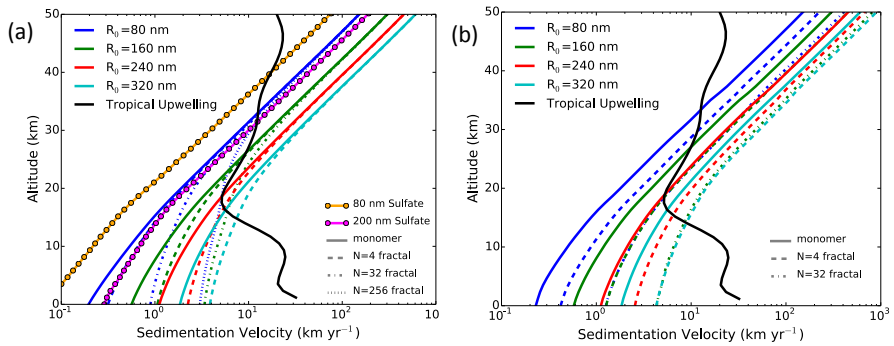


Figure 1. Annual average sedimentation velocity (km yr$^{-1}$) versus altitude for (a) uncoated alumina particles and pure sulfate particles and (b) sulfate-coated aged alumina paticles with compact fractal structures averaged over the region from 20°S to 20°N latitude. Solid colored lines represent monomers, dashed lines fractals with N=4, dash-dot lines fractals with N=32, and dotted lines fractals with N=256 (for $R_0$=80 nm only). Fractal dimension $D_f$=1.6 for uncoated particles represented in panel (a), $D_f$=2.8 for coated and compacted particles shown in panel (b). The black lines represent the annual average upwelling velocity of the model's advective transport averaged over the region from 20°S to 20°N latitude for comparison.

Debra Weisenstein 8/11/2015 4:36 PM
**Deleted:** S

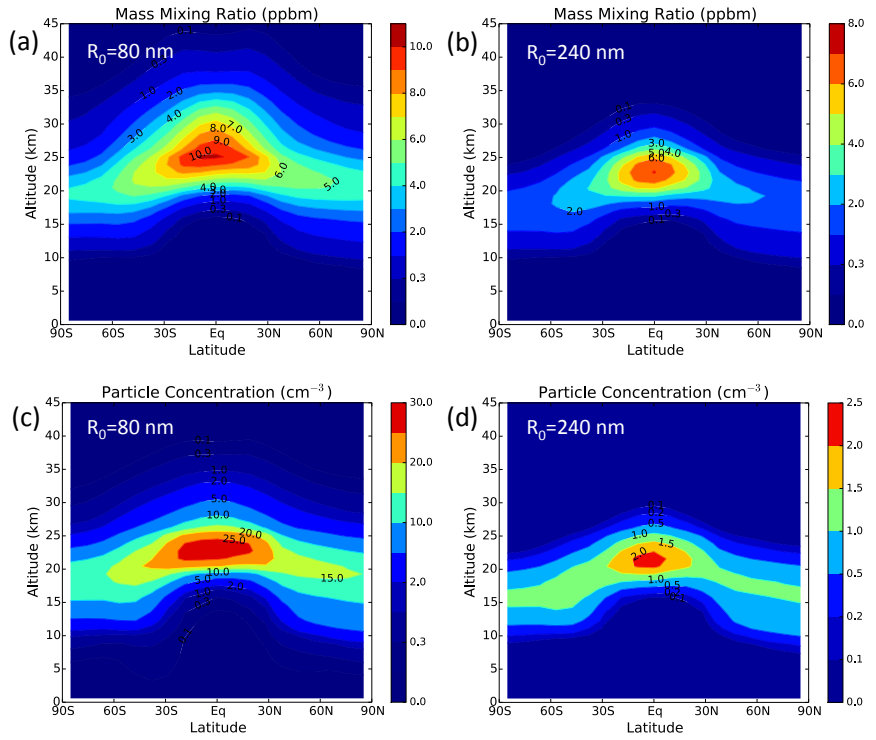


Figure 2. Mass mixing ratio of alumina in ppbm (panels a and b) and number density of alumina particles in $cm^{-3}$ (panels c and d) with geoengineering injections of 1 Tg $yr^{-1}$ of 80 nm monomers (panels a and c) and 1 Tg $yr^{-1}$ of 240 nm monomers (panels b and d) for annual average conditions.

Debra Weisenstein 6/17/2015 3:38 PM
**Deleted:** Concentration

Debra Weisenstein 7/21/2015 12:48 PM
**Deleted:** Mt yr

Debra Weisenstein 7/21/2015 12:48 PM
**Deleted:** Mt yr

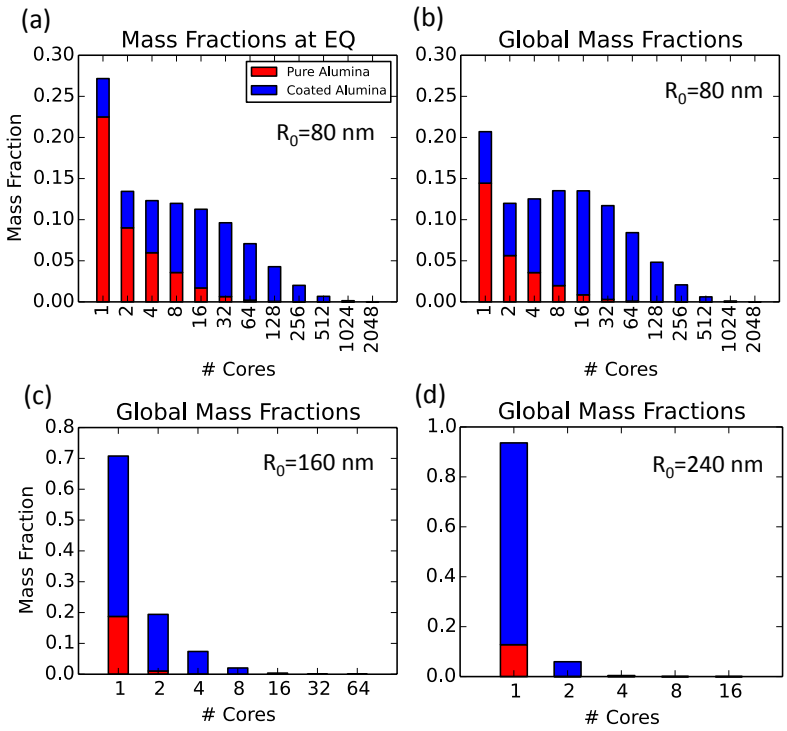


Figure 3. Distribution of integrated stratospheric alumina mass into monomers and fractals for geoengineering injection of 1 Tg $yr^{-1}$ of alumina as 80 nm monomers at (a) the equator and (b) globally integrated, and for injection of 1 Tg $yr^{-1}$ of alumina as (c) 160 nm and (d) 240 nm monomers globally integrated. Red bar length represents the mass fraction in dry alumina and blue bar length the mass fraction in coated alumina. Annual average conditions are represented.

Debra Weisenstein 7/21/2015 12:48 PM
**Deleted:** Mt yr

Debra Weisenstein 7/21/2015 12:48 PM
**Deleted:** Mt yr

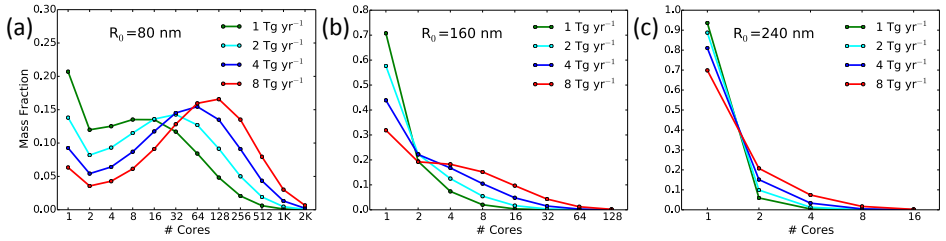


Figure 4. Calculated global annual average stratospheric mass fractions of alumina as a function of the number of monomers contained in a fractal particle for (a) monomer injections of 80 nm radius, (b) monomer injections of 160 nm, and (c) monomer injections of 240 nm radius, with emission rates ranging from 1 to 8 Tg $yr^{-1}$.

Debra Weisenstein 7/21/2015 12:48 PM
**Deleted:** Mt yr

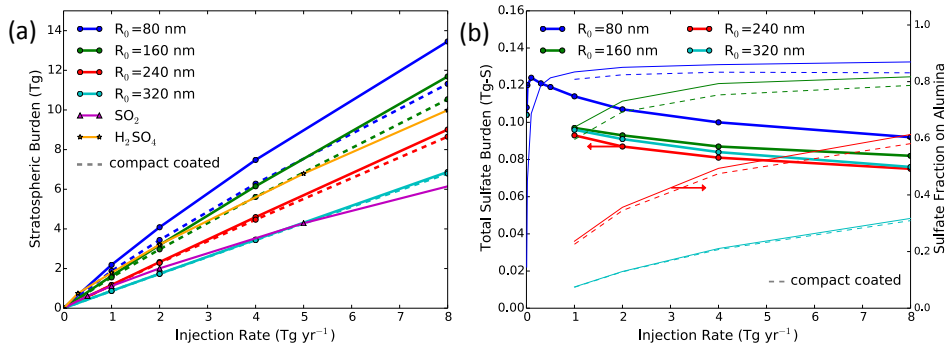


Figure 5. Annual average stratospheric burden of (a) alumina and (b) condensed sulfate versus injection rate for various sizes of injected alumina monomers. For comparison, we plot sulfate burden in Tg-S as a function of the rate of injection of $SO_2$ and $H_2SO_4$ (Pierce et al., 2010) in Tg-S yr$^{-1}$ along with alumina burden in (a). Panel (b) shows the fate of natural sulfate as a function of alumina injection rate, where the total sulfate burden is plotted on the left-hand axis (thick lines with circles) and the fraction of that burden that is on the alumina particles is shown on the right-hand axis (thin lines). The dashed lines represent simulations in which the coated alumina particles are assumed to become more compact in shape.

Debra Weisenstein 7/28/2015 5:58 PM
**Deleted:** S

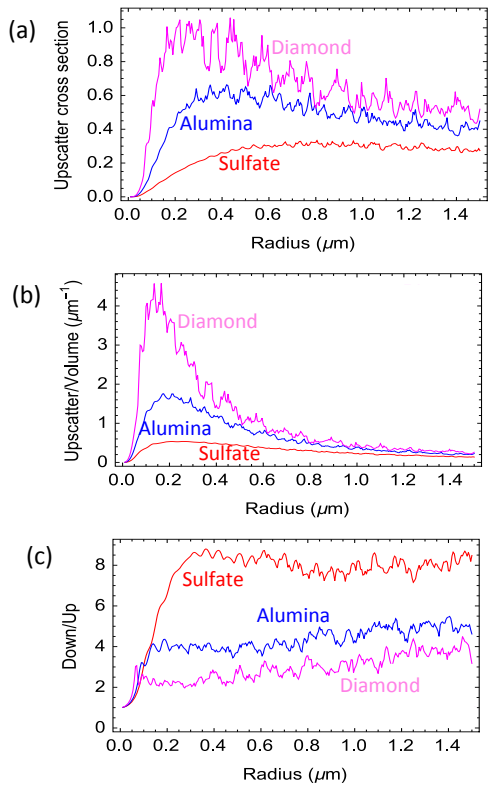


Figure 6. Comparison of radiative scattering properties of alumina and diamond monomers and sulfate aerosol particles as functions of particle radius. Panel (a) shows the upscatter cross-section divided by the geometric cross-section (a dimensionless ratio). Panel (b) shows the upscatter cross-section divided by the particle volume (units of $\mu m^{-1}$), and panel (c) shows the ratio of downscatter cross-section to upscatter cross-section integrated over the solar band.

Debra Weisenstein 7/21/2015 2:43 PM
**Deleted:** s

Debra Weisenstein 7/21/2015 2:44 PM
**Deleted:** per unit

Debra Weisenstein 7/21/2015 2:45 PM
**Deleted:**

Debra Weisenstein 7/21/2015 2:45 PM
**Deleted:**

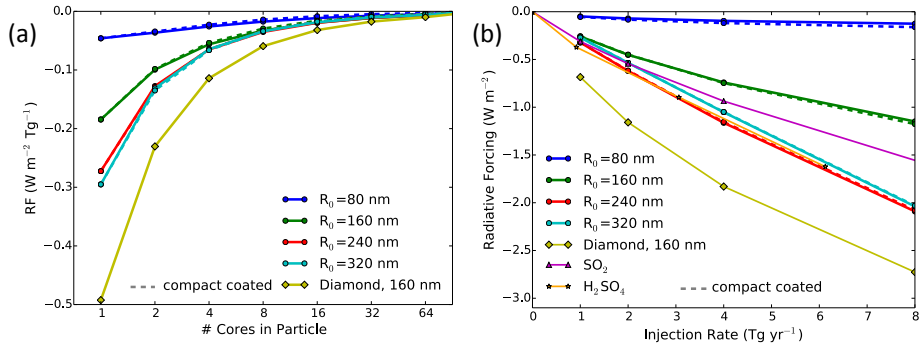


Figure 7. Shortwave globally-averaged clear-sky radiative forcing per terragram burden (W m$^{-2}$ Tg$^{-1}$) of alumina or diamond particles as a function of the number of monomer cores per fractal particle (panel a). Calculated globally-averaged shortwave radiative forcing as a function of injection rate for geoengineering scenarios (panel b) for annual average cloud-free conditions. The dashed lines represent simulations in which the coated alumina particles are assumed to become more compact in shape.

Debra Weisenstein 7/24/2015 10:12 PM
**Deleted:** R

Debra Weisenstein 7/24/2015 10:27 PM
**Deleted:** megaton

Debra Weisenstein 7/26/2015 11:54 PM
**Deleted:** globally-averaged

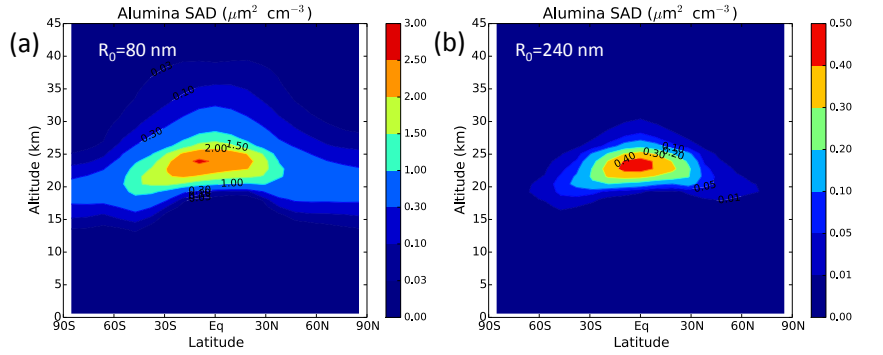


Figure 8. Calculated annual average surface area density (μm$^2$ cm$^{-3}$) of uncoated alumina particles due to geoengineering with 1 Tg yr$^{-1}$ injection of (a) 80 nm alumina monomers and (b) 240 nm alumina monomers.

Debra Weisenstein 7/21/2015 12:48 PM
**Deleted:** Mt yr

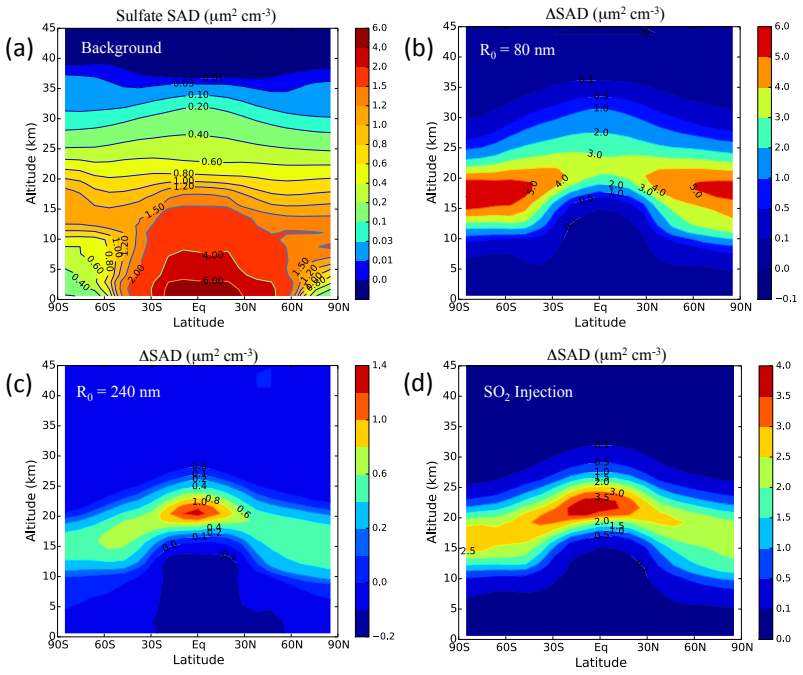


Figure 9. Calculated annual average sulfate surface area density ($\mu m^2$ $cm^{-3}$) of (a) sulfate particles without geoengineering, and surface area density increase ($\mu m^2$ $cm^{-3}$) with geoengineering injections of (b) 1 Tg $yr^{-1}$ of 80 nm alumina monomers and (c) 1 Tg $yr^{-1}$ of 240 nm alumina monomers. Panel (d) shows sulfate aerosol surface area density increase ($\mu m^2$ $cm^{-3}$) with 1 Tg $yr^{-1}$ of $SO_2$ injection.

Debra Weisenstein 7/21/2015 12:48 PM
**Deleted:** Mt yr

Debra Weisenstein 7/21/2015 12:48 PM
**Deleted:** Mt yr

Debra Weisenstein 7/21/2015 12:48 PM
**Deleted:** Mt yr

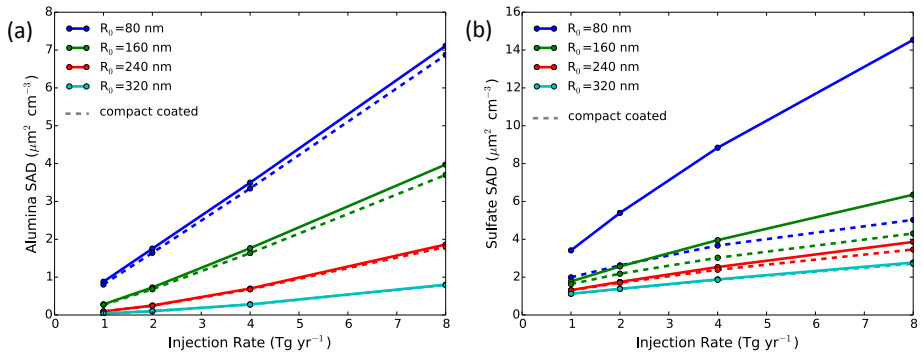


Figure 10. Global annual average stratospheric surface area density between 15 and 25 km altitude for (a) uncoated alumina, and (b) total sulfate. The dashed lines represent simulations in which the coated alumina particles are assumed to become more compact in shape.

Debra Weisenstein 8/20/2015 3:36 PM
**Deleted:** A

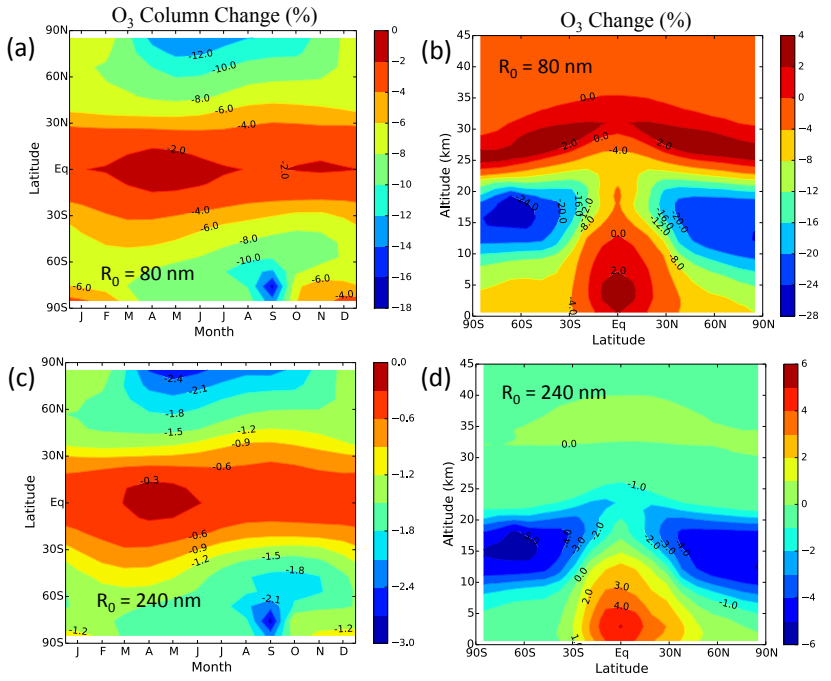


Figure 11. Ozone changes due to injection of alumina aerosol. Column ozone changes (%) are shown as a function of latitude and month (left panels) and annual average local ozone changes (%) as a function of latitude and altitude (right panels). Results are shown for an injection rate of 1 Tg $yr^{-1}$ of 80 nm (top panels) and 240 nm (bottom panels) alumina monomers. Note ozone increases in the upper stratosphere where the $NO_x$ cycle dominates and decreases in the lower stratosphere where the $ClO_x$ and $BrO_x$ cycles dominate.

Debra Weisenstein 7/21/2015 12:48 PM
**Deleted:** Mt yr

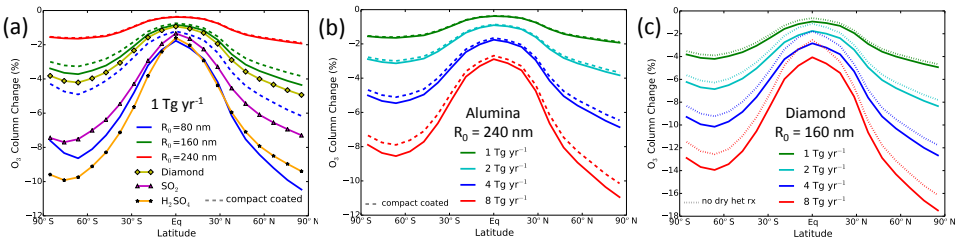


Figure 12. Annual average column ozone change in percent as a function of latitude for (a) cases with 1 Tg $yr^{-1}$ injections of alumina monomers of 80 nm, 160 nm, and 240 nm, and diamond monomers of 160 nm and $SO_2$ and $H_2SO_4$, (b) cases with injection of 240 nm alumina monomers at rates of 1, 2, 4, and 8 Tg $yr^{-1}$, and (c) cases with injection of 160 nm diamond monomers at rates of 1, 2, 4, and 8 Tg $yr^{-1}$. Cases in which coated particles are assumed to become more compact in shape are shown with dashed lines in panels (a) and (b). For diamond, cases without reaction (R1) occurring on dry diamond particle surfaces are shown with dotted lines in panel (c).

Debra Weisenstein 7/21/2015 12:48 PM
**Deleted:** Mt yr

Debra Weisenstein 8/11/2015 4:41 PM
**Deleted:** alumina

Debra Weisenstein 8/11/2015 4:41 PM
**Deleted:** as

Debra Weisenstein 7/21/2015 12:48 PM
**Deleted:** Mt yr

Debra Weisenstein 7/21/2015 12:48 PM
**Deleted:** Mt yr

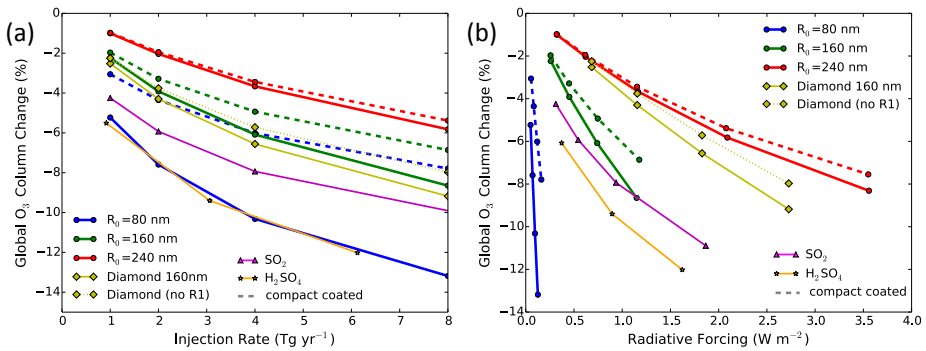


Figure 13. Global annual average column ozone change (in percent) (a) as a function of injection rate and (b) as a function of associated radiative forcing. Ozone change for diamond is shown with and without reaction (R1) on uncoated diamond particles. Calculations with $SO_2$ and $H_2SO_4$ injections employ the same model to calculate radiative forcing and ozone depletion as for alumina and diamond.

Debra Weisenstein 8/20/2015 3:39 PM
**Deleted:** as